Spatiotemporal dynamics of RAD51C between the Golgi and nucleus regulates homologous recombination and genomic stability.

George Galea[1*]†, Karolina Kuodyte[1,2]†, Muzamil M. Khan[1,3], Peter Thul[4], Beate Neumann[5], Emma Lundberg[4,6,7], Rainer Pepperkok[1,3,5*]

[1] Cell Biology and Biophysics Unit, European Molecular Biology Laboratory (EMBL), 69117 Heidelberg, Germany
[2] Collaboration for joint PhD degree between EMBL and Heidelberg University, Faculty of Biosciences
[3] Translational Lung Research Center Heidelberg (TLRC), German Center for Lung Research (DZL), Heidelberg, Germany
[4] Science for Life Laboratory, School of Engineering Sciences in Chemistry, Biotechnology and Health, KTH - Royal Institute of Technology, Stockholm, 17121, Sweden.
[5] Advanced Light Microscopy Facility, EMBL, Heidelberg, 69117, Heidelberg, Germany
[6] Department of Bioengineering, Stanford University, Stanford, CA 94305, USA
[7] Department of Pathology, Stanford University, Stanford, CA 94305, USA

† These authors contributed equally.
* Corresponding authors: george.galea@embl.de; rainer.pepperkok@embl.org

Abstract

Intra-organelle communication is essential for cellular homeostasis, but the coordination between nuclear processes and cytoplasmic compartments remains poorly understood. Here, we uncover a novel spatiotemporal regulatory pathway linking the Golgi complex to the nucleus upon DNA damage. We show key DNA repair proteins, including RAD51C, dynamically shuttle between these organelles in response to distinct types of DNA damage. Mechanistic analysis reveals that RAD51C is anchored at the Golgi by Giantin. Disrupting this interaction leads to premature RAD51C nuclear localization, impaired homologous recombination signaling, genomic instability, and increased cell proliferation. Our findings establish Golgi-nuclear communication as a critical regulator of DNA repair, offering new insights into genomic integrity maintenance with profound implications for cancer and aging-related genomic instability.

Introduction

Eukaryotic cells have evolved a highly specialised and coordinated array of membrane-bounded organelles. This compartmentalisation allows the segregation of biochemical reactions, ensuring that they are carried out with the highest specificity and efficiency. However, organelles do not function in isolation but rely on the continual exchange of lipids, proteins and signalling cues to maintain cellular homeostasis. At the centre of this cross-coordination of subcellular transport and signalling pathways lies the Golgi complex. Thus, contributing well beyond its classical roles of membrane trafficking, and post-translational modification but also acting as a regulatory hub with numerous cellular processes intersecting at this organelle such as autophagy, mitosis, growth signalling, cytoskeletal and energy status regulation (*1*, *2*). Perturbations to the Golgi architecture and mutations of its constituents have been associated with a wide array of human diseases such as neurodegenerative disorders and cancer, amongst many others (*3*–*6*). Although we have a clearer picture of the Golgi's interactions and regulatory functions in the cytoplasmic domain, its communication with thel nucleus remains largely unexplored.

Emerging themes have started to illustrate the relationship between the Golgi and nuclear compartment, with multi-localisation proteins playing a pivotal role. For example, in cholesterol homeostasis and ER stress response, sensing-signalling proteins SREBP and ATF6, respectively, get proteolytically cleaved at the Golgi complex to regulate gene expression through the release of a transcriptionally active amino terminus that makes its way to the nucleus (*7*, *8*). Few studies have also hinted at a link between cytoplasmic organelles, genomic stability, and, in turn, cancer, with the Golgi complex emerging as a central theme (*9*–*11*). At a structural level, the Golgi undergoes dramatic morphological changes following the induction of DNA lesions, from ribbon-like perinuclear stack to dispersed fragments (*12*). A response requiring the phosphorylation of the Golgi resident oncoprotein, Golgi phosphoprotein 3 (GOLPH3), by DNA-dependent protein kinase (DNA-PK), aDNA Damage Response (DDR) regulator (*12*). Golgi morphology alterations are also a common feature across a wide variety of cancer types and are often reflected in changes in the distribution of Golgi resident proteins (*9*, *11*). Rearrangement of Golgi glycosyltransferases distribution is a recurrent phenomenon in cancer cells, resulting in defective glycosylation, a process thought to promote cancer development (*9*, *11*, *13*). These

studies hint at a clear link between Golgi and nucleus as communicating organelles, however a systematic approach that could pin down the signalling pathways involved in this communication has been missing.

To this end, here, we utilise localisation data and antibody resources from the Human Protein Atlas (HPA) project (*14*) to explore a class of multi-localisation proteins as a systematic strategy to identify key signalling pathways that function between the Golgi and nuclear compartment. Our work reveals the first example of a network of DNA repair proteins localised to the Golgi complex. We systematically analyse their subcellular localisation within the Golgi, as well as their redistribution patterns in response to various types of DNA damage. Furthermore, we propose a novel spatiotemporal regulatory pathway for DDR control between the Golgi complex and nucleus, activating Homologous Recombination (HR)-mediated DNA repair. Our findings reveal that the spatial localisation of RAD51C between the Golgi and nucleus is critical for proper HR function. We demonstrate that Giantin is crucial for the Golgi localisation of RAD51C, while GMAP210-mediated localisation of NBN at the Golgi is necessary for recruiting RAD51C to the nucleus upon DNA double-strand break (DSB) induction. The dysregulation of RAD51C by depletion of Giantin leads to genomic instability, impaired DDR signalling, and increased cell proliferation, highlighting the critical role of spatial regulation of DDR proteins in maintaining genomic integrity and cellular homeostasis. This work opens up an exciting new scientific niche with the potential to identify novel therapeutic targets.

Results

Antibody-based systematic analysis identifies a network of DNA damage response proteins at the Golgi complex.

To systematically explore possible candidates that link Golgi to nuclear function or vice versa, we shortlisted 329 proteins identified by the Human Protein Atlas (HPA) project (*14*) to localise at both Golgi-like membranes and the cell nucleus **(Fig. 1A)**. siRNA-mediated validation experiments (*15*) confirmed the double-localisation of 163 candidates (167 antibodies) **(Fig. 1B; Supplementary table S1)**.

Bioinformatic analysis of the identified 163 candidates revealed a number of functional protein networks **(Fig. 1B)**, primarily composed of two major pathways: membrane trafficking and surprisingly, DNA repair **(Fig. 1B and C)**. Additionally, we identified enrichment for cell cycle regulation, RNA metabolism, and lipid metabolism regulators **(fig. S2B and Supplementary Table S1)**. Within the membrane trafficking enriched cluster, we identified several essential components of intra-Golgi trafficking machinery, including Golgins, SNAREs, COG tethering complex, and RAB GTPase exchange factors **(Fig. 1B)**.

An enriched cluster centred on the DNA Damage Response (DDR) emerged through the combination of DNA repair proteins and an array of cell cycle regulators (**Fig. 1D; fig. S1 & fig. S2A and B**). Within this cluster, we identified various proteins collectively spanning the core DNA repair pathways (Homologous Recombination (HR); Mismatch Repair (MMR); Microhomology-Mediated End Joining (MMEJ) and Base Excision Repair (BER)) as well as other integral regulators of DDR such as ubiquitination, cell cycle and signalling **(Fig. 1D and**

144 **E)**. These surprising findings of DNA repair proteins at the Golgi prompted us to explore the
145 links between DDR and Golgi function.
146
147 **Golgi cisternal localisation analysis of dual-localising DDR proteins identifies specific**
148 **distribution patterns that correlate with their function.**
149
150 To start addressing the role of DDR proteins at the Golgi complex, we shortlisted 15
151 candidates based on their described role in this pathway and conducted an in-depth analysis
152 of their subcellular distribution within the organelle. The Golgi apparatus consists of *cis*-,
153 *medial*, and *trans*-Golgi cisternae, extending into a tubular *trans*-Golgi network (TGN), with
154 resident Golgi proteins strategically distributed along the Golgi stack in order to serve their
155 function (*10*). Employing confocal microscopy, we characterised the relative localisation of
156 the dual-localising DDR proteins within the Golgi. Using a *cis*-Golgi marker, GM130, and a
157 *trans*-Golgi marker, TGN46, we performed a cross-correlation analysis of the distribution
158 patterns of DDR proteins at the Golgi **(Fig. 2A to E**; **fig. S3D; Supplementary Table S2**)
159 (*16*). DDR proteins were found to be distributed into three major localisation patterns
160 throughout the Golgi cisternae: a subset co-localising predominantly with the *trans*-Golgi
161 marker, TGN46 **(Fig. 2A, B and E**), a second subset co-localising with the *cis*-Golgi marker,
162 GM130 **(Fig. 2C, D and E**) and a third subset not having a strong preference for either
163 marker. Remarkably, these distribution patterns appear to correlate with the DDR pathways
164 in which these proteins participate (**Fig. 2E**). Although the limited number of proteins
165 identified so far prevents us from drawing definitive conclusions, there are notable trends.
166 For example, BER and MMEJ proteins TOPORS, LIG1, and POLQ exhibited co-localisation
167 with the *trans*-Golgi marker, TGN46, while HR factors NBN and RAD51C have a high
168 correlation with the *cis*-Golgi marker, GM130.
169
170 **Dual-localising DDR proteins dynamically redistribute between the Golgi and nucleus**
171 **in response to specific types of DNA injuries.**
172
173 We next examined whether Golgi-nuclear localising DDR proteins respond to DNA damage,
174 focusing on two genotoxic stressors: Double-Strand DNA Breaks (DSBs) and oxidative
175 stress. We induced the formation of DSBs by utilising doxorubicin (DOX), a widely used
176 therapeutic known to interact with DNA by intercalation (*17*), while oxidative DNA damage
177 was induced by hydrogen peroxide (H_2O_2) (*18*) or potassium bromate ($KBrO_3$) (*19*) **(Fig. 2F**
178 **to H; fig. S3 to S5**).
179
180 Using this experimental approach we monitored for any genotoxic stress-induced changes
181 in protein distribution pattern of the 15 Golgi-nuclear localising DDR proteins. Initial visual
182 inspection of these experiments revealed that all three genotoxic treatments induced
183 significant changes in both the subcellular localisation patterns and protein levels of the
184 majority of the tested candidates. Two predominant protein redistribution patterns were
185 observed, either in a Golgi-to-nuclear manner or conversely, in a nucleus-to-Golgi direction.
186 Additionally, we documented variations in the total fluorescence levels across numerous
187 candidates. In this context, we observed instances of both decrease or increase in the protein
188 levels for multiple candidates. To capture these changes quantitatively, we measured the
189 fluorescence levels in both the Golgi and nuclear compartments and then calculated a Golgi-
190 nuclear distribution ratio for each protein. This ratio provides a robust and quantitative
191 measurement of Golgi-nuclear distribution, while also accounting for potential protein level

192 fluctuations due to treatment or population heterogeneity. A ratio value below 1 signifies a
193 shift from Golgi-to-nucleus, whereas a value above 1 indicates nucleus-to-Golgi
194 redistribution.
195
196 The quantifications of the Golgi-nuclear ratio revealed a correlation between the redistribution
197 patterns of these DDR proteins and their subcellular distribution with the Golgi complex.
198 Here, treatment with DOX **(Fig. 2F and G; fig. S3**) resulted in a predominantly uniform
199 localisation pattern change, where *cis*-Golgi DDR proteins (3 out of 4) shifted from the Golgi
200 to the nucleus, whereas *trans*-Golgi proteins (7 out of 8) displayed a redistribution pattern
201 from the nucleus to the Golgi. Conversely, exposure to H_2O_2 or $KBrO_3$ **(Fig. 2F and H; fig.**
202 **S4 and S5**) elicited the opposite response, with the majority of *trans*-Golgi DDR proteins (7
203 out of 8) displaying a redistribution from the nuclear compartment to the Golgi while 2 out of
204 the 4 *cis*-Golgi DDR proteins displayed a redistribution pattern from the nucleus to the Golgi.
205
206 When examining these proteins within the context of their associated DNA repair pathways,
207 a distinct trend also emerged. Proteins participating in BER (TOPORS and LIG1) and MMEJ
208 (POLQ) exhibited opposing redistribution patterns compared to the MMR regulator (MSH6)
209 and HR proteins (RAD51C and NBN) **(Fig. 2G; fig. S3)**. Specifically, with DOX treatment,
210 BER and MMEJ proteins shifted from the nucleus to the Golgi, while MMR and HR proteins
211 relocated from the Golgi to the nucleus. Conversely, this trend was reversed with H_2O_2 or
212 $KBrO_3$ treatments **(Fig. 2H; fig. S4 and S5)**.
213
214 **Redistribution of RAD51C Golgi fraction is required for the formation of RAD51C repair**
215 **nuclear foci and is dependent on the kinase ATM.**
216
217 To mechanistically dissect the novel link between the Golgi complex and the nucleus, we
218 characterised the Homologous Recombination (HR) repair protein RAD51C. As a member
219 of the RAD51 paralog family, RAD51C is essential for regulating HR-mediated repair of
220 double-strand breaks (DSBs). Various studies have demonstrated RAD51C's involvement
221 across multiple stages of HR repair: promoting the DNA damage checkpoint (*20*), aiding in
222 RAD51 filament formation, stabilising replication forks, and resolving Holliday junctions to
223 complete repair (*21–23*). This versatility in function, combined with a significant Golgi-
224 localised population compared to other DNA damage response (DDR) proteins, prompted us
225 to investigate RAD51C as an ideal candidate for understanding how Golgi-associated DDR
226 proteins might facilitate dynamic recruitment to various repair complexes. RAD51C contains
227 both a nuclear localisation signal (NLS) and a nuclear export signal (NES) (*24*), which may
228 enable it to shuttle between the Golgi and the nucleus in response to DNA damage, thereby
229 supporting its role in replication fork stabilisation and HR repair.
230
231 Following the validation of RAD51C localisation, we confirmed these results using antibodies
232 targeting different RAD51C epitopes across several cell lines (**Fig. 3A and B**). Our
233 observations revealed distinct subcellular localisation distribution for exogenous RAD51C.
234 We identified a juxta-nuclear compact localisation (**indicated by the yellow arrowhead**) co-
235 localised with the Golgi marker, GM130. Additionally, RAD51C displayed a dispersed nuclear
236 distribution with distinct foci (**highlighted by the white arrowhead**) and a diffused cytosolic
237 distribution. The specificity of the antibodies was confirmed by the depletion of RAD51C (**fig.**
238 **S6A to C**). To biochemically validate the subcellular localisation of RAD51C, we isolated
239 nuclear, membrane and cytoplasmic fractions from HeLa Kyoto (HK) protein extracts and

240 probed them for RAD51C presence in each compartment (**Fig. 3C and D**). The protein was
241 found to be present in all fractions with the majority of the protein being present in the
242 membrane and cytoplasmic compartment, in agreement with our immunofluorescence data.
243
244 Having already established that RAD51C localisation changes with the introduction of DSBs
245 (**Fig. 2G; fig. S3**), we investigated the temporal dynamics of this redistribution by monitoring
246 RAD51C localisation over time following treatment with DOX. Upon drug addition (**Fig. 3E to**
247 **H**), we observed an overall decrease in RAD51C protein level, with the Golgi-localised
248 fraction (co-localised with GM130, **yellow arrows**) decreasing more rapidly than the nuclear
249 fraction. Concurrently, the diffused nuclear RAD51C pattern changed into very distinct
250 nuclear foci (**white arrows**), which become more pronounced with longer DOX exposure
251 (**Fig. 3E**).
252
253 Quantitative analysis of these experiments allowed us to measure the changes in RAD51C
254 levels at both the Golgi (**Fig. 3F**) and the nuclear compartment (**Fig. 3G**), and to calculate a
255 RAD51C Golgi-nuclear distribution ratio (**Fig. 3H**). This redistribution was further validated
256 by subcellular fractionation (**Fig. 3I**; **fig. S6D**). Similarly, the total protein level of RAD51C is
257 observed to decrease after 3 h treatment, with a much larger reduction in the membrane
258 compartment when compared to the nuclear fraction. Additionally, we observed an increase
259 in RAD51C cytoplasmic fraction with DOX treatment. Overall, in both experiments, the
260 RAD51C Golgi-nucleus distribution ratio is seen to decrease significantly after 3 h DOX
261 treatment in both the immunofluorescence and biochemical assay (**Fig. 3H and I).**
262
263 To identify a mechanism for RAD51C redistribution between compartments, we induced
264 DSBs using DOX while inhibiting Importin-β-mediated nuclear import with the small peptide
265 inhibitor Importazole (IPZ) (*25*). IPZ treatment (**Fig. 3J to L, fig. S7A; Golgi fraction**
266 **marked with yellow arrows; nuclear foci marker with white arrows**) inhibited the DOX-
267 induced RAD51C redistribution. Instead, the majority of the protein population remained co-
268 localised with the Golgi marker, GM130, and nuclear foci formation was significantly inhibited
269 **(Fig. 3J)**. While a reduction in the overall RAD51C protein level was measured with DOX
270 treatment alone, no significant change in the RAD51C distribution pattern was observed with
271 IPZ treatment (**fig. S7A)**.
272
273 We next sought to test whether the phosphorylation of DDR kinases mediates RAD51C
274 redistribution in response to DSBs. The three master kinases that are active in response to
275 DNA damage are ataxia-telangiectasia mutated (ATM), Ataxia telangiectasia and Rad3-
276 related (ATR) and DNA-dependent protein kinase (DNA-PK) (*26*). Cells were treated with
277 phosphorylation inhibitors specific for each kinase and RAD51C redistribution was analysed
278 following DOX treatment (**Fig. 3M to O; fig. S7B; Golgi fraction marked with yellow**
279 **arrows**).
280
281 DOX combined with the ATM phosphorylation inhibitor, KU55933 (*27*) significantly inhibited
282 RAD51C redistribution, with the majority of the protein remaining co-localised with GM130
283 and nuclear foci formation blocked **(Fig. 3M)**. In contrast, the combined treatment of DOX
284 with ATR or DNA-PK phosphorylation inhibitors, VE-821 (*28*) and NU7441 (*29*) respectively,
285 had no apparent impact on the redistribution of RAD51C when compared with cells treated
286 with DOX only**.** Additionally, inhibitor-only treatments did not alter RAD51C localisation (**fig.**
287 **S7B**).

To confirm that these observations were a direct result of DSBs and not an off-target drug effect, we tested other DSB-causing agents (*30*): camptothecin (CPT) (**fig. S8A to C**), etoposide (ETO) (**fig. S8D to F**), and mitomycin C (MMC) (**fig. S8G to I**). All treatments led to significant RAD51C redistribution from the Golgi to the nuclear compartment. Notably, CPT treatment (**fig. S8A**) caused a shift in nuclear RAD51C from a **diffuse distribution to distinct foci**, while ETO or MMC treatments (**fig. S8D and G**) increased the nuclear RAD51C population without obvious foci formation.

Golgi localisation of RAD51C and NBN is dependent on the Golgins Giantin and GMAP210, respectively.

To identify potential Golgi membrane anchors for RAD51C, we analysed data from two genome-wide siRNA screens aimed at identifying regulators of HR and DDR (*31*, *32*). Interestingly these studies highlighted the Golgin protein family as potential candidate genes, where the knockdown of Giantin and GMAP210 led to a significant reduction in HR repair rates (*32*) (**Golgin results summarised in fig. S9A**), and the depletion of Giantin significantly inhibited H2AX phosphorylation, a crucial event in DDR signalling regulation (*31*) (**Golgin results summarised fig. S9B**). Given the structural properties of Golgins (**Fig. 4A**), which are predominantly coiled-coil proteins anchored to the Golgi membrane by their carboxy terminus and projected into the surrounding cytoplasm (*33*), they are ideally suited for capturing or tethering nearby membranes and potentially retaining DDR proteins such as RAD51C.

To investigate whether RAD51C localisation is dependent on these Golgins, we performed siRNA-mediated depletion of Giantin and GMAP210, and compared their effects on RAD51C distribution to a control siRNA treatment (**Fig. 4B to E**). GMAP210 depletion had no significant effect on RAD51C distribution, whereas Giantin knockdown led to a notable redistribution of RAD51C (**Fig. 4B**). Specifically, we observed a marked decrease in RAD51C co-localisation with the Golgi marker GM130 (**yellow arrows**) and an increase in nuclear RAD51C localisation with distinct bright nuclear foci appearing (**white arrows**) (**Fig. 4B**). Quantifications revealed a significant reduction of the RAD51C Golgi population, (**Fig. 4C**) and the distribution ratio (**Fig. 4D**) reduced by more than half. The number of RAD51C foci (**Fig. 4E**) increased by more than two-fold upon depletion of Giantin with either siRNAs. There was no significant difference in either RAD51C Golgi intensity, distribution ratio or foci number (**Fig. 4C to E**) between the GMAP210-depleted and control cells. The effective knockdown of Giantin (**fig. S9C**) and GMAP210 was tested by immunofluorescence. Sub-Golgi cisternae localisation analysis confirmed that Giantin and RAD51C are distributed in a similar manner throughout the organelle (**Fig. 4F and G**).

To determine if RAD51C physically interacts or forms a complex with Giantin we performed an immunoprecipitation (IP) assay (**Fig. 4H and I**). . Endogenous Giantin and RAD51C were found to co-IP from HK protein extracts (**Fig. 4H**). To explore the dynamics of this interaction in response to DNA damage, we induced DSBs and performed co-IP experiments (**Fig. 4I**). Our results showed that RAD51C and Giantin dissociate upon DSB induction. However, co-treatment with either an ATM inhibitor or IPZ, alongside doxorubicin, prevented this dissociation, corroborating our earlier immunofluorescence observations (**Fig. 3E to O**).

336 To gain insight into the nature of RAD51C foci induced by Giantin depletion, we carried out
337 co-localisation assays to determine whether these structures contain standard HR markers,
338 phosphorylated H2AX (γ-H2AX) (**Fig. 4J and K**) and phosphorylated ATM (p-ATM) (**Fig. 4L**
339 **and M**) under physiological conditions and induction of DSBs by ETO. Both proteins are well-
340 established markers for DSB repair sites and are important for the recruitment of the HR
341 repair machinery (*34*). In cells treated with a control siRNA, we observed that approximately
342 half of the RAD51C nuclear foci were decorated with either γ-H2AX or p-ATM (**Fig. 4J to M**;
343 **colocalising foci are denoted with an arrow**), as previously described (*34*). RAD51C foci
344 induced by the depletion of Giantin however showed significantly lower co-localisation with
345 both markers both with or without the induction of DSBs. Overall, Giantin-depleted cells
346 showed fewer γ-H2AX and p-ATM nuclear foci, consistent with previous reports (*31*) (**fig.**
347 **S9B**).
348
349 Having confirmed that RAD51C Golgi localisation depends on Giantin, we tested whether the
350 other identified HR factor at the Golgi, NBN (also known as NBS1 or Nibrin), is similarly
351 dependent on Giantin or GMAP210. While Giantin depletion did not affect NBN distribution,
352 GMAP210 knockdown caused a significant reduction in the NBN Golgi population (**yellow**
353 **arrow; Fig. 4N and O)**. Specifically, NBN co-localisation with GM130 decreased to about
354 one-third of the original level **(yellow arrows)**. No significant differences were seen in
355 Giantin-depleted cells. We further confirmed an interaction between NBN and GMAP210
356 through IP assays (**Fig. 4P**). Endogenous NBN and GMAP210 co-immunoprecipitated in
357 HeLa Kyoto extracts, supporting their functional association.
358
359 **GMAP210 anchors NBN at the Golgi, facilitating ATM-mediated phosphorylation and**
360 **RAD51C release**
361
362 NBN is a critical regulator of HR (*35*) and is essential for recruiting RAD51C to nuclear foci
363 during the DDR (*20*). Given its pivotal role in initiating and activating ATM and HR pathways,
364 we hypothesised that the Golgi-localised population of NBN might be crucial for the
365 redistribution of RAD51C from the Golgi to the nucleus following DSB induction.
366
367 Since knockdown of NBN disrupts the ATM and HR signalling, complicating our analysis, we
368 instead targeted its Golgi anchor, GMAP210, and examined the effects on RAD51C
369 recruitment (**Fig. 5A to C**). Under control conditions, RAD51C redistributes from the Golgi to
370 the nucleus upon DSB induction (**Fig. 5A; yellow arrows denote the Golgi**). However, in
371 GMAP210-depleted cells, this redistribution was blocked, resulting in the retention of
372 RAD51C at the Golgi and a diminished nuclear population. These findings suggest that
373 GMAP210 and potentially NBN are required for RAD51C's release from Giantin and
374 subsequent nuclear translocation, likely involving a complex where these proteins are in
375 close proximity. To explore this further, we tested whether endogenous GMAP210 and
376 Giantin interact through co-IP (**Fig. 5D**). The results confirmed their interaction, suggesting
377 they may be part of a larger DDR Golgi complex.
378
379 NBN is a known substrate of ATM (*36*), and that ATM activity is crucial for RAD51C's release
380 from the Golgi, we hypothesised that ATM mediates this release via NBN phosphorylation at
381 the Golgi. To test this, we investigated the presence of ATM at the Golgi membranes through
382 a biochemical Golgi enrichment approach (**Fig. 5E to G**). By fractionating and enriching *cis*-
383 and *trans*-Golgi fractions, we detected ATM in the *cis*-Golgi fraction under control conditions,

384 (**Fig. 5E**) with phosphorylated ATM (pATM) appearing after DSB induction (**Fig. 5F and G**).
385 Anticipating that ATM would be proximal to Giantin, we performed a co-IP experiment to
386 determine if ATM is part of a complex with Giantin (**Fig. 5H**). Our results confirmed that ATM
387 co-IP with Giantin, further supporting the notion that ATM is active on the Golgi membranes
388 to facilitate the release of RAD51C.
389
390 To further substantiate this, we monitored ATM activity during early DSB induction by staining
391 for phosphorylated SQ/TQ motifs, which recognise ATM/ATR substrates, we observed
392 increased phosphorylation of these substrates in both the nucleus and the Golgi after 30
393 minutes of DSB induction (**Fig. 5I**). Although this phosphorylation was more prominent in the
394 nucleus, there was a significant increase at the Golgi as well (**denoted by yellow arrows**).
395 We then investigated whether NBN is phosphorylated at the Golgi (**Fig. 5J**). After inducing
396 DSBs for 30 minutes, we observed an increase in phosphorylated NBN (pNBN S343)
397 predominantly at the nucleus with a lesser but still significant increase at the Golgi (**denoted**
398 **by yellow arrows**). To determine whether NBN phosphorylation at the Golgi depends on
399 GMAP210, we conducted GMAP210 knockdown and monitored NBN phosphorylation levels
400 at the Golgi under steady-state conditions and after DNA damage induction. In all conditions,
401 we observed a significant reduction of NBN phosphorylation at the Golgi (**Fig. 5K; fig. S9D;**
402 **yellow arrows denote the Golgi**).
403
404 Finally, we investigated whether this phosphorylation is ATM-dependent and requires nuclear
405 signal transduction (**Fig. 5L; fig. S9D; yellow arrows denote the Golgi**). Using an ATM
406 inhibitor and blocking nuclear export with leptomycin B (LMB) (*37*), we observed a significant
407 reduction of NBN phosphorylation at the Golgi under both control conditions and after DNA
408 damage induction. These results suggest that the NBN population anchored by GMAP210 is
409 phosphorylated by ATM as a crucial step in facilitating the release of RAD51C from the Golgi.
410
411 **Spatial dysregulation of RAD51C by depletion of Giantin leads to genomic instability,**
412 **inhibition of ATM signalling and accelerated cell proliferation.**
413
414 To determine whether the spatial dysregulation of RAD51C, NBN, and potentially other HR
415 factors by Giantin and GMAP210 depletion influences genomic stability and DNA repair, we
416 first measured the incidence of micronuclei formation (**Fig. 6A and B**), a standard biomarker
417 for genotoxic damage (*38*). Depletion of Giantin or RAD51C significantly increased the
418 percentage of cells displaying micronuclei and aberrant nuclear structures compared to
419 controls, while GMAP210 knockdown had no significant effect (**Fig. 6B**).
420
421 To further confirm that Giantin depletion compromises genomic integrity, we performed
422 comet assays (*39*) to measure levels of fragmented genomic DNA (**Fig. 6C and D**). Cells
423 with defective DNA repair or exposed to DNA-damaging agents display long comet tails,
424 whereas healthy cells show shorter or no tails. Knockdown of Giantin or RAD51C resulted in
425 notably longer comet tails compared to control siRNA treatment (**Fig. 6C**). Quantification
426 revealed a 2.5-fold increase in tail length and fluorescence intensity for RAD51C-depleted
427 cells, and 1.8- to 1.6-fold increases for Giantin-depleted cells (siGiantin#1 and siGiantin#2,
428 respectively) (**Fig. 6D**).
429
430 Having established that Giantin depletion leads to genomic instability, we next examined the
431 long-term consequences on cell proliferation and colony formation in HK and U-2 OS cells

(**Fig. 6E to H**). Giantin knockdown significantly enhanced both proliferation and colony formation. To determine whether these effects were associated with cell cycle changes, we analysed the cell cycle profiles of Giantin-depleted cells via FACS (**fig. S9E**). No significant cell cycle alterations were detected, suggesting that the increased proliferation is not due to major cell cycle perturbations.

Given the critical roles that DDR proteins interacting with Giantin and GMAP210 play in HR activation and DNA repair, their spatial dysregulation could significantly impact HR signalling. To explore this, we assessed the ability of cells depleted of Giantin and GMAP210 to initiate HR by measuring ATM phosphorylation, the master regulator of this pathway (**Fig. 6I and J**). In control siRNA treated cells, DOX treatment increased phosphorylated ATM levels in response to DSBs. However, Giantin-depleted cells (**Fig. 6I**) showed significantly lower ATM phosphorylation levels under the same conditions, whereas GMAP210 depletion (**Fig. 6J**) had no observable effect on ATM activation.

To investigate whether the redistribution of HR factors from the Golgi to the nucleus plays a role in ATM signalling, we used Importazole (IPZ) to inhibit Importin-β-mediated nuclear import and subsequently induced DSBs with doxorubicin (DOX) (**Fig. 6K**). Here, we found that IPZ treatment did not significantly alter ATM signalling, regardless of the induction of DSBs. These findings suggest that the regulated redistribution of HR factors is less impactful on ATM signalling than their mislocalisation, implying that Giantin's spatial regulation of HR factors is crucial for proper ATM activation, whereas GMAP210's role may operate downstream within the DDR pathway.

To further substantiate the role of RAD51C spatial dysregulation in ATM signalling inhibition, we conducted co-depletion of RAD51C and Giantin, along with individual depletions (**Fig. 6L and M**). Consistent with previous observations, Giantin knockdown led to a significant decrease in ATM phosphorylation levels, while RAD51C knockdown increased ATM phosphorylation. Interestingly, co-depletion of RAD51C and Giantin restored ATM phosphorylation levels to those comparable to control cells. To validate the restoration of DDR signalling through co-depletion, we assessed genomic stability via micronuclei incidence (**Fig. 6N**). Individual knockdowns of Giantin and RAD51C elevated micronuclei formation, indicative of genomic instability, whereas co-depletion significantly reduced micronuclei incidence, approaching levels observed in control cells. Lastly, we evaluated cell proliferation (**Fig. 6O**). While Giantin knockdown enhanced cell proliferation and RAD51C knockdown diminished it, co-depletion resulted in proliferation rates comparable to control, further highlighting the interplay between these proteins in regulating cellular responses to DNA damage.

Discussion

In this study, we reveal a novel and significant spatiotemporal regulatory system connecting the Golgi complex and the nucleus, with direct implications for homologous recombination (HR) and other DNA repair pathways. Our analysis of Human Protein Atlas (HPA) localisation data (*14*) and experimental validation via siRNA knockdowns uncovered a surprisingly high number of double-localising Golgi-nuclear proteins. Among these, we identified a cluster of DNA repair proteins that exhibit steady-state localisation in both compartments. This cluster

480 encompasses crucial regulatory proteins involved in various DNA repair pathways (**Fig. 1D**),
481 not only specific for HR-mediated DNA repair but also Mismatch Repair (MMR), Base
482 Excision DNA Repair (BER) and Microhomology-Mediated End Joining (MMEJ), as well as
483 other integral regulators of DNA repair cellular responses such as chromatin cohesion,
484 ubiquitination, cell cycle regulation and signalling. To our knowledge, this is the first report
485 demonstrating a DNA repair protein network that localises to both the Golgi complex and the
486 nucleus, potentially linking Golgi-associated cytoplasmic events to DNA repair pathways.
487
488 Our systematic analysis revealed that these DNA repair proteins are enriched in distinct sub-
489 Golgi regions. This suggests a compartmentalised platform where components of related
490 DNA repair pathways gather, potentially facilitating protein–protein interactions and
491 enhancing the specificity of downstream signaling. The enriched association of the Golgins
492 Giantin and GMAP210 with HR factors, suggesting a structural or scaffolding role in
493 organising these repair proteins. These Golgi-resident proteins may stabilise DDR factors at
494 the Golgi and help regulate their release to the nucleus. The close association between
495 Golgins and DNA repair kinases, such as ATM, further supports the notion that the Golgi can
496 orchestrate finely tuned phosphorylation events. Through these events, DDR proteins might
497 be properly assembled and activated before being dispatched to DNA lesions. This spatial
498 organisation likely preserves pathway fidelity by preventing premature or ectopic activation
499 of repair proteins and by supporting the timely recruitment of DDR components.
500
501 In response to genotoxic stress, we observed dynamic shuttling of DNA repair factors
502 between the Golgi and the nucleus, dependent on the type of DNA damage. The correlation
503 between DDR protein localisation pattern at the Golgi and their redistribution patterns upon
504 DNA damage underscores the Golgi's role in temporally coordinating DDR activation. We
505 propose that the Golgi clusters DDR proteins during steady-state conditions and releases
506 them to the nucleus when damage is detected. This mechanism ensures that repair proteins
507 are delivered to DNA lesions at the right time and context, regulating protein stoichiometry,
508 optimizing repair efficiency and fidelity**.** The dynamic localisation of these proteins parallels
509 the behaviour of known shuttling proteins like BRCA1, whose movement between the
510 nucleus and cytoplasm modulates its roles in DNA repair, cell cycle regulation, and apoptosis
511 (*40–42*). Similarly, Golgi-mediated spatiotemporal regulation of RAD51C, NBN, and other
512 DDR proteins may be essential for maintaining genomic stability and potentially linking Golgi-
513 associated cytoplasmic events.
514
515 To dissect this spatiotemporal regulation, we detailed a pathway linking the Golgi to HR repair
516 (**Fig. 6P**). Based on our findings and existing literature, we propose that the pathway begins
517 with the detection of double-strand DNA breaks (DSBs) in the nucleus by the MRN complex,
518 which activates ATM kinase. ATM then transduces the signal to the Golgi membranes, where
519 it phosphorylates the Golgi population of NBN. Anchoring of NBN by GMAP210 at the Golgi
520 supports a structural role for Golgins in facilitating this signal transduction. Our data suggest
521 an organelle-based checkpoint mechanism wherein ATM phosphorylates the Golgi-localised
522 NBN, which in turn triggers the release of RAD51C from Giantin. This ensures a
523 spatiotemporal gating of HR factors based on the damage context. The presence of ATM on
524 the Golgi membranes supports the idea that phosphorylation events occur in a spatially
525 controlled manner at the Golgi before repair proteins are dispatched to the nucleus. Our data
526 suggest that Importin-β or active recycling between the Golgi and nucleus may facilitate this
527 spatiotemporal release of RAD51C. This mechanism is consistent with the previously

528 observed function of importin-α at the Golgi, which competes with p115 for interaction with
529 the Golgin GM130, regulating vesicle fusion and Golgi disassembly during mitotic
530 progression (*43*, *44*). Once released, RAD51C, potentially with its binding partners,
531 translocates to DNA damage sites to engage in HR and regulate DDR signaling.
532
533 Disruption of this finely-tuned system through Giantin depletion leads to the premature
534 release of RAD51C into the nucleus. This mislocalisation bypasses the regulated mechanism
535 involving ATM-dependent phosphorylation of NBN, resulting in defective HR signalling.
536 Without the spatial and temporal control imposed by the Golgi, RAD51C may not assemble
537 correctly into functional repair complexes or may arrive at damage sites without proper
538 activation cues. Consequently, HR efficiency is compromised, leading to increased genomic
539 instability and uncontrolled cell proliferation. These findings align with previous studies
540 showing that knockdowns of Giantin and GMAP210 inhibit HR repair rates (*32*) and interfere
541 with H2AX phosphorylation (*45*).
542
543 RAD51C is a pivotal component of the RAD51 paralog complexes BCDX2 and CX3,
544 executing essential roles in stabilising replication forks, promoting RAD51 filament assembly,
545 and resolving Holliday junctions (*46*, *47*). Consequently, its mislocalisation undermines these
546 processes, impairing the recruitment of repair factors and DDR signalling with downstream
547 effects on other factors such as CHK2 (*20*, *48*). Importantly, several interconnected
548 mechanisms explain why mislocalisation of RAD51C produces such strong phenotypic
549 consequences. As a central member of HR, RAD51C orchestrates RAD51 filament formation
550 and subsequent strand invasion steps essential for faithful DSB repair (*21*, *49*). If prematurely
551 released to the nucleus or improperly retained at the Golgi, RAD51 filaments may be
552 disorganised or suboptimally assembled, leading to error-prone repair events. RAD51C also
553 influences checkpoint signaling by stabilising replication forks and interacting with ATR–RPA,
554 enabling proper CHK2 phosphorylation and cell-cycle arrest upon DNA damage (*20*, *50*).
555 Dysregulation of these checkpoint pathways can encourage cells to progress through the cell
556 cycle despite harboring DNA lesions. The Golgi appears to act as a "coordinator" that
557 maintains correct stoichiometry of RAD51C and potentially other RAD51 paralogs until ATM-
558 mediated phosphorylation of NBN signals a controlled release. Bypassing this spatial gating
559 results in faulty HR complex assembly at damage sites, culminating in replication stress,
560 chromosome aberrations, and proliferative advantages often associated with oncogenesis.
561
562 The link between Golgin dysfunction (particularly Giantin) and elevated breast cancer risk
563 (*51*–*56*), as well as decreased patient survival (**fig. S9F and G**) (*57*, *58*) underscores the
564 clinical importance of Golgi-regulated DDR. The involvement of other Golgin family members
565 in various cancers (*59*, *60*) further suggests a broad role for Golgi scaffolding and signaling
566 processes in controlling genomic integrity. These observations raise the intriguing possibility
567 of exploiting Golgi-based DDR regulation as a biomarker or therapeutic target in cancer
568 management.
569
570 Finally, our observation that many other proteins dually localise to the Golgi and nucleus—
571 spanning membrane trafficking, RNA metabolism, and lipid regulation—suggests the Golgi
572 is a dynamic integration hub for multiple essential pathways. Its newly recognised role in
573 DNA repair orchestration may extend beyond HR to additional DDR networks. Altogether,
574 these findings encourage a reevaluation of how the Golgi contributes to genome

575 maintenance and cell proliferation control, opening new avenues for both fundamental
576 research and translational approaches in DNA repair and cancer biology.
577
578
579 **Materials and Methods**
580
581 **Antibodies and chemicals.** Several commercially antibodies and chemical were used in the
582 paper, including RAD51C (ab72063, Abcam; 1:500 for immunostaining) & (ab95069, Abcam,
583 1:2000 for western blotting; 1:500 for immunoprecipitation), GOLGB1/Giantin (AF8159, R&D
584 systems; 1:500 for immunostaining and immunoprecipitation, 1:2000 for western blotting) &
585 (G1/M1, Enzo Life Sciences, 1:500 for immunostaining), GM130 (610822, BD Biosciences;
586 1:500 for immunostaining, 1:2000 for western blotting), TGN46 (AHP500GT, Bio-Rad; 1:1000
587 for immunostaining; 1:2000 for western blotting), ATM (MA1-23152, Invitrogen; 1:2000 for
588 western blotting), ATM (MA1-23152, Invitrogen, 1:1000 for western blotting), pATM Ser1981
589 (MA1-2020, Invitrogen; 1:500 for immunostaining; 1:2000 for western blotting), CHK2 pThr68
590 (PA5-17818, Invitrogen; 1:2000 for western blotting), DNA-PKcs (Ser2056) (PA5-78130,
591 Invitrogen, 1:2000 for western blotting), gamma-H2AX pSer139 (613402, Biolegend; 1:500
592 for immunostaining, 1:2000 for western blotting), alpha-tubulin (MS-581, Thermo Fisher;
593 1:10,000 for western blotting) Lamin B1 (ab16048, Abcam; 1:2000 for western blotting)
594 vinculin (ab219649, abcam; 1:2000 for western blotting), HSP60 (ab46798, abcam; 1:10000
595 for western blotting), MRE11 (NB100-142, Novus Biologicals; 1:2000 for western blotting);
596 pSer343 NBN (ab226066, abcam; 1:500 for immunostaining; 1:2000 for western bloting), p-
597 (Ser/Thr) ATM/ATR Substrate (#2851, Cell signalling; 1:500 for immunostaining),
598 doxorubicin (ab120629, Abcam); Importazole (SML0341, Sigma-Aldrich), KU55933 (ATMi,
599 SML1109, Sigma-Aldrich); ve-821 (ATRi, HY-14731; MedChemExpress) NU7441 (DNA-PKi,
600 HY-11006; MedChemExpress), etoposide (ab120227, Abcam), mitomycin C (M7949, Sigma-
601 Aldrich), hydrogen peroxide (H1009, Sigma-Aldrich), potassium bromate (104912, Merck
602 Millipore), camptothecin (ab120115, Abcam), SYBR Gold (S11494, Invitrogen), crystal violet
603 (C0775-100G, Sigma-Aldrich).
604
605 **Cell lines, cell culture and siRNA transfection.** HeLa Kyoto, U-2 OS, MCF7, were cultured
606 in DMEM (Life Technologies) supplemented with 10% FBS (Invitrogen) and 1% L-glutamine
607 (Invitrogen). Cells were checked for mycoplasma contamination by PCR. siRNA transfections
608 were performed with Lipofectamine 2000 (Invitrogen) using SilencerSelect siRNAs (Ambion)
609 according to the manufacturer's instructions. Transfections were carried out for 72 h and the
610 final siRNA concentrations used were 15nM for all siRNAs. Giantin siRNA-1: 5951 & siRNA-
611 2: 5953; GMAP210 siRNA-1: s17811 & siRNA-2: s17812; RAD51C siRNA: s11737; ATM
612 siRNA: s532284; NBN siRNA: s9291.
613
614 **Localisation validation siRNA assay**. A custom-designed siRNA library targeting our
615 proteins of interest (Ambion) was designed and prepared in 96-well glass bottom plates
616 (Miltenyi Biotec) using a protocol for solid phase reverse transfection as previously described
617 (*15*, *61*). Non-targeting siRNA was used as a negative control. 72 hours after cell seeding,
618 cells were fixed with 4% paraformaldehyde (PFA), permeabilised with 0.1% Triton-X100 and
619 immunostained against the HPA antibodies of interest and a Golgi marker, GM130. Hoechst
620 33342 was used as a nuclear stain. siRNAs and antibodies details are available in
621 Supplementary Table S1. Images were acquired on a fully automated Molecular Devices IXM
622 with a 10x/0.45 NA P-APO objective. The resulting images were analysed using Cell Profiler

software (*62*) for quantitative and automated measurements of fluorescence from the antibodies as previously described (*15*). Briefly, nuclei were segmented in the nuclear channel, the Golgi complex was segmented in the Golgi marker channel and using the segmented nuclei as seeds, the two structures were associated. Intensity profiles of each compartment were acquired. A reduction of 25% or more of the antibody staining in both Golgi and nuclear compartments was considered as a validation of the antibody specificity **(fig. S1 and S2; Supplementary Table S1)**.

Golgi cisternal localisation analysis. As previously described (*16*), HK cells were treated with nocodazole (33 μM) or the solvent control methanol for 3 h. After treatment, cells were fixed with 4% PFA, permeabilized with 0.1% Triton-X100 and immunostained using antibodies against *trans*-Golgi marker, TGN46, *cis*-Golgi marker, GM130 and the protein of interest. Images of the Golgi mini-stacks were acquired using a confocal microscope Olympus Fluoview FV3000 with a 60x/1.3 NA silicon oil immersion apochromatic objective. Golgi mini-stacks were visually inspected, and those that were in the same plane were selected for analysis. Images were analysed using Fiji (*63*); the relative position of the fluorescence profile of the protein of interest against the *trans*- and *cis-Golgi* markers was measured using a plot profile tool. The measured distances were used to calculate Pearson's correlation coefficient (PCC) between *cis*-Golgi and *trans*-Golgi markers and proteins of interest.

Drug treatments. Cells were treated 24 h after seeding. For camptothecin, etoposide and mitomycin C experiments, cells were treated for 16 h at a concentration of 0.1 μM, 50 μM and 5 μM, respectively. After treatment cells were incubated with fresh medium for 2 hours. H_2O_2 experiments were performed by treating cells for 20 min at a concentration of 50 μM, followed by change with fresh medium and 15 min recovery. For nocodazole and $KBrO_3$ experiments cells were treated for 3 h at the concentration of 33 μM and 5 mM, respectively. Doxorubicin was used at a concentration of 40 μM for 3 h unless indicated otherwise. For kinase and importin-β inhibitor treatments, cells were pretreated for 30 min with the described inhibitor prior to the addition of doxorubicin. The inhibitors were used at the following concentrations: importazole (IPZ) (20 μM), KU55933 (ATMi) (30 μM), NU7441 (DNA-Pki) (10 μM) and ve-821 (ATRi) (10 μM).

Immunofluorescence assay. Cells were fixed with 4% paraformaldehyde in PBS and permeabilised with 0.1% Triton X-100 for 15 min at room temperature, then cells were blocked with 5% bovine serum albumin in 0.05% Triton X-100 for 60 min and incubated with primary antibodies in blocking buffer at room temperature for 3 h. Following 3 washes with PBS, cells were incubated with fluorescent dye-conjugated secondary antibodies diluted in a blocking buffer for 1 h at room temperature.

Image and data analysis. Confocal microscopy experiments were performed with fixed and immunostained cell samples on a microscope FV3000, Olympus. Z stacks of images covering the entire cell thickness were acquired. All image analysis was performed using Cell Profiler (*62*) and Fiji (*63*). Briefly, first nuclei were segmented in the Hoechst channel. When appropriate, the Golgi complex was segmented in the Golgi marker channel and using the segmented nuclei as seeds, the two structures were associated. Intensity profiles, morphology features and structuring counting analysis were performed when required using Cell Profiler.

671
672 **Comet assay.** The assay was carried out as previously described (*64*). Briefly, cells were
673 trypsinised, pelletised and resuspended in ice-cold PBS at a concentration of 25 × 10^4 cells
674 per ml. The cells were resuspended in 2% low melting agarose (Sigma) and spread quickly
675 onto gel bond film (Biozym) covered in 1% agarose (Sigma). Samples were immersed into a
676 lysis buffer (100 mM EDTA, 2.5 M NaCl, 10 mM Tris-HCl and 1% Triton-X100; pH 10)
677 overnight at 4°C. Followed by a wash with ice-cold water and run in an electrophoresis
678 chamber (alkaline buffer: 1 mM EDTA, 300 mM NaOH; pH 13) at 15 V, 300 mA for 60 min at
679 4°C. Slides were first washed in a Tris-HCl neutralisation buffer (0.4 M; pH 7.5) followed by
680 water, stained with SYBR Gold (Thermo Fisher Scientific) (1:10000) and finally dried. Comets
681 were imaged by an automated Olympus Scan^R screening microscope and comet tails were
682 scored using OpenComet plugin (*65*).
683
684 **Western blotting analysis.** HK cells were lysed using RIPA buffer (Thermo Scientific) with
685 a complete protease inhibitor cocktail (Roche). SDS-PAGE was performed on pre-cast Tris-
686 Acetate gels followed by transfer to PVDF transfer membrane (Merck Millipore). Proteins
687 were detected using primary antibodies as described followed by incubation with secondary
688 antibodies coupled with HRP (Invitrogen). Detection of protein was performed using Pierce
689 ECL Plus Western Blotting Substrate reagent (Thermo Scientific) and visualised on Azure
690 280 chemiluminescent imaging system. Golgi enrichment assay was performed using
691 Minute™ Golgi Apparatus Enrichment Kit (GO-037, Invent Biotechnologies) according to the
692 manufacturer's instructions. The purity of the cis and trans-Golgi fractions was confirmed by
693 using Golgi markers GM130 for the *cis*-Golgi and TGN-46 for the *trans*-Golgi. Subcellular
694 fractionation was performed using a subcellular protein fractionation kit for cultured cells
695 (78840, Thermo Scientific) according to the manufacturer's instructions. Fractions were
696 verified using well-established markers (GM130 for Golgi membranes, Lamin B1 for the
697 nuclear compartment, and alpha-tubulin for the cytoplasmic fraction) and probed for proteins
698 of interest presence in each compartment. Protein membrane:nuclear distribution ratio was
699 calculated by first dividing the protein level in each fraction by the protein level of the
700 appropriate control, the resulting membrane ($M_{protein}$ / M_{GM130}) and nuclear ($N_{protein}$ / $N_{laminB1}$)
701 ratios were further divided to give the ratio = ($M_{protein}$ / M_{GM130}) / ($N_{protein}$ / $N_{laminB1}$). The ratios
702 obtained from the control were normalised to 1 and compared to the treated group.
703
704 **Immunoprecipitation.** HK cells were lysed using a lysis buffer (50 mM Hepes, 130 mM
705 NaCl, 1 mM DTT 1% NP-40) with a complete protease inhibitor cocktail (Roche). Cell lysates
706 were centrifuged at 13,000 rpm for 10 mins at 4°C. For immunoprecipitation, the lysates were
707 incubated with the primary antibody described and rotated overnight at 4°C. Next, the lysates
708 were incubated with G-agarose beads (Roche) and rotated for 4 h at 4°C. The samples were
709 washed with cold lysis buffer and then precipitated proteins were eluted by 2x SDS sample
710 buffer and analysed by Western blotting.
711
712 **Colony formation assay.** HK or U-2 OS cells, transfected with either a Giantin or control
713 siRNA were seeded on a 6-well plate (500 cells/well) and allowed to grow for 12 days in a
714 complete culture medium. Where indicated, 24h after seeding the cells were treated with a
715 DNA damaging agent, DOX (1 μM) or a solvent control, DMSO for 24h. Subsequently, the
716 medium was replaced, and it was refreshed every 4 days. The resulting colonies were
717 washed twice with PBS, followed by fixing and staining for 30 min with a solution containing
718 0.1% (w/v) crystal violet and 20% (v/v) ethanol. Then the colonies were washed again to

remove excess crystal violet with PBS. Finally, after the dishes were dry, digital images of the colonies were acquired using a camera and quantified.

Statistical analysis. All data were obtained from at least three independent experiments if not otherwise stated. Statistical analyses were performed using a two-tailed t-test for pairwise comparison and one-way analysis of variance (ANOVA) for multiple comparisons on GraphPad Prism 9. Data are expressed as the standard error of the mean (s.e.m.). n values indicate biologically independent samples and experiments. $P < 0.05$ was considered statistically significant.

Acknowledgements. We thank the ALMF, FCCF and the Pepperkok team for their support. In addition, we acknowledge Jan Ellenberg, Claudia Lukas, Alba Diz-Muñoz, Diana Ordonez, Per Haberkant and Simone Köhler for their assistance in developing the project and manuscript. G.G. was supported by the EMBL EIPOD programme, K.K. by the EMBL PhD programme and M.M.K. by the German Centre for Lung Research.

Figure legends

Fig. 1. Antibody-based analysis identifies a network of DNA damage response (DDR) proteins at the Golgi complex. (**A**) Schematic diagram of the screening process for the shortlisting, validation and characterisation of Golgi-nuclear localisation proteins, as a strategy to identify linking pathways. (**B**) Experimentally-based protein-protein interaction network displaying the DNA repair and membrane trafficking Golgi-nuclear localisation proteins validated in this study; categorised by functional pathways. (**C**) Pathway enrichment analysis of the Golgi-nuclear localisation proteins identified in this study. (**D**) Experimentally-based STRING protein-protein interaction network showing the DDR proteins identified to localise to both the Golgi complex and nucleus; yellow nodes indicate double-localising proteins, and grey nodes are filler untested proteins. (**E**) Representative images of HeLa Kyoto cells stained with antibodies against Golgi-nuclear DDR proteins (green), and the Golgi marker GM130 (red). DNA was stained with Hoechst 33342 (blue). Yellow arrowheads denote the Golgi complex. Scale bar, 10 µm.

Fig. 2. Systematic analysis of Golgi-nuclear localisation DDR proteins. (**A** to **E**) Golgi-cisternal localisation analysis of Golgi-nuclear DDR proteins. HK cells were treated with Nocodazole (33 µM, 3 h), fixed and stained with antibodies against DDR proteins. (**A** and **C**) Enlarged view of single isolated mini-stack, where cells were stained with antibodies against TOPORS, CCAR1 and Golgi markers GM130 (*cis*-Golgi) and TGN46 (*trans*-Golgi); scale bar, 1 µm; (**B** and **D**) white lines across the stack depict the line-plot analysis. (**E**) Quantification of Pearson's correlation coefficient (PCC) between *cis*-Golgi and *trans*-Golgi markers and DDR proteins; $n \geq 36$ mini-stacks. (**F**) Localisation changes of dual-localising DDR proteins upon induction of DNA damage. HK cells were treated with the DNA damage-inducing drug, doxorubicin (DOX) (40 µM, 3 h) or oxidative stress-inducing agent hydrogen peroxide (H_2O_2) (50 µM for 20 min, followed with 15 min recovery), fixed and stained with antibodies against DDR proteins LIG1, POLQ, CCAR1 and the Golgi marker, GM130; yellow arrows denote the Golgi membranes. Scale bars, 10 µm. (**G**) A ratio of DDR protein Golgi-nuclear distribution after treatment with DOX and (H) H_2O_2. Data represent the mean ± standard error of the

766 mean (s.e.m.) ($n = 3$ biologically independent samples with at least 200 cells analysed for
767 each protein in control and treatment conditions). The proteins are classified according to
768 their Golgi localisation patterns (**E**). Statistical significance was determined using a two-tailed
769 unpaired Student's *t*-test; ns P > 0.05, **P < 0.01, ***P < 0.001, ****P <0.0001, compared to
770 untreated control.
771
772 **Fig. 3. Redistribution of RAD51C Golgi fraction is required for the formation of RAD51C**
773 **nuclear foci and is dependent on the kinase ATM.** (**A**) Representative images of HK, U-2
774 OS and MCF7 cells stained with antibodies against RAD51C (green) and GM130 (red). DNA
775 stained with Hoechst 33342 (blue). (**B**) Quantification of RAD51C distribution across the
776 Golgi, nucleus and cytoplasm in various cell lines quantified from immunofluorescence
777 images. (**C**) WB analysis showing the subcellular membrane (M), nuclear (N) and
778 cytoplasmic (C) fractions of RAD51C (markers: GM130 for Golgi membranes, Lamin B1 for
779 the nuclear compartment, alpha-tubulin for the cytoplasmic fraction). (**D**) Quantification of
780 western blot analysis showing the distribution of RAD51C in 3 cell fractions: membrane,
781 nuclear and cytoplasmic; ($n = 3$ biologically independent experiments) data represent the
782 mean ± s.e.m. (**E**) HK cells treated with the DNA damage-inducing drug, doxorubicin (DOX),
783 for increasing lengths of time. Yellow arrows denote the Golgi membrane; white arrows
784 denote nuclear foci. (**F**) Quantification of sum intensity of RAD51C Golgi population, (**G**)
785 RAD51C nuclear population, and (**H**) a ratio of RAD51C Golgi-nuclear distribution after
786 treatment with DOX. Data represent the s.e.m ($n = 3$ biologically independent samples with
787 a total of 2343 cells analysed). (**I**) Quantification of RAD51C membrane-nuclear distribution
788 ratio after treatment with DOX, calculated from isolated fractions (fig. S6E). HK cells were
789 stained with antibodies against RAD51C and GM130. (**J**) Cells were treated with DMSO or
790 IPZ prior to a 3-hour treatment with DOX. Yellow arrows denote the Golgi membrane; white
791 denote nuclear foci. Results were quantified as (**K**) ratio of RAD51C Golgi-nuclear distribution
792 and (**L**) relative sum intensity of RAD51C at the Golgi Data represents s.e.m. ($n = 3$
793 biologically independent samples with a total of 445 cells analysed). (**M**) HK cells were
794 treated with DMSO (control) alone or with ATM inhibitor (KU55933) or ATR inhibitor (VE-821)
795 or DNA-PK inhibitor (NU7441) prior to a 3-hour treatment with doxorubicin. Results were
796 quantified as (**N**) ratio of RAD51C Golgi-nuclear distribution and (**O**) relative sum intensity of
797 RAD51C at the Golgi. Data represents s.e.m. ($n = 3$ biologically independent samples with a
798 total of 1679 cells analysed). Scale bars, 10 μm. Statistical significance was determined using
799 a two-tailed unpaired Student's *t*-test.
800
801 **Fig. 4. RAD51C and NBN Golgi localisation is dependent on the Golgin proteins Giantin**
802 **and GMAP210, respectively.** (**A**) Graphical representation of Giantin protein configuration.
803 (**B**) HK cells transfected with control or Giantin siRNAs for 72 hours, stained with antibodies
804 against RAD51C and Golgi marker GM130. Yellow arrows indicate the Golgi and white
805 arrows indicate nuclear foci. Quantification of the localisation changes of RAD51C quantified
806 as (**C**) relative sum intensity of RAD51C at the Golgi, (**D**) fluorescent intensity ratio of the
807 RAD51C Golgi-nuclear distribution and (**E**) relative number of RAD51C foci per cell. Data
808 represent the mean ± s.e.m. ($n = 3$ biologically independent samples with a total of 1445 cells
809 analysed). (**F**) Golgi-cisternal co-localisation analysis. HK cells treated with Nocodazole (33
810 μM, 3 h), fixed and stained with antibodies against Giantin and RAD51C. (**G**) Zoom enlarged
811 view of single isolated mini-stack; scale bar, 1 μm; white line across the stack was used for
812 line-scan analysis. (**H**) Immunoprecipitation of endogenous Giantin and RAD51C under
813 control conditions and (**I**) after treatment with DOX or co-treatments ATMi and IPZ from HK

814 cell extracts. (**J** to **M**) Co-localisation experiment of cells treated with control siRNA, or Giantin
815 siRNA under control conditional or after treatment with ETO. Cells stained with antibodies
816 against RAD51C (green) and HR DDR markers (red): (**J**) γ-H2AX, and (**L**) p-ATM. Co-
817 localisation of structure is denoted by an arrowhead. Quantification of percentage RAD51C
818 foci co-localising with (**K**) γ-H2AX and (**M**) p-ATM. Data represent the mean ± s.e.m. ($n = 3$
819 biologically independent samples with at least 200 cells and at least 550 RAD51C nuclear
820 foci analysed for the co-localisation experiments for each condition). (**N**) HK cells were
821 transfected with control, Giantin or GMAP210 siRNAs for 72 hours and stained with
822 antibodies against NBN and Golgi marker, GM130. Yellow arrows indicate the Golgi. (**O**)
823 Quantification of the localisation changes of NBN were quantified as relative sum intensity of
824 NBN at the Golgi and nucleus. (**P**) Co-immunoprecipitation of endogenous GMAP210 and
825 NBN. Statistical significance was determined using a two-tailed unpaired Student's *t*-test.
826 Scale bars, 10 μm.
827
828 **Fig. 5. GMAP210 is required for RAD51C nuclear redistribution in response to DSBs.**
829 (**A**) HK cells transfected with control or GMAP210 siRNAs and treated with solvent control
830 DMSO or ETO (10 μM), stained with antibodies against RAD51C and Golgi marker, GM130.
831 Yellow arrows indicate the Golgi. RAD51C redistribution changes after treatment with ETO
832 were quantified for (**B**) the Golgi and (**C**) nuclear compartment. (**D**) Co-immunoprecipitation
833 of endogenous Giantin with GMAP210 from HK cell extracts. (E to G) Western blot analysis
834 of HK *cis*- and *trans*-Golgi enriched protein fractions, probing for (**E**) ATM, and (**F**) pATM
835 under control conditions and (**G**) pATM after treatment with DOX (40 μM) (markers: GM130
836 for *cis*-Golgi, TGN46 for *trans*-Golgi, HSP60 for mitochondria, H2AFX for nuclei). (**H**) Co-
837 immunoprecipitation of endogenous Giantin with ATM from HK cell extract. (**I** and **J**) HK cells
838 treated with solvent control, DMSO or ETO (10 μM) for 30 min. Cells stained with antibodies
839 against GM130 and (**I**) phosphorylated SQ/TQ (pS/TQ) motifs, which recognise ATM/ATR
840 substrates, the intensity of the image was intentionally increased, resulting in some structures
841 being oversaturated. This was done to enhance the visibility of Golgi signal; (**J**) pNBN (S343).
842 Yellow arrows indicate the Golgi. Quantification of the relative change in NBN
843 phosphorylation level at the Golgi in response to (**K**) GMAP210 depletion, (**L**) nuclear export
844 block by leptomycin B (LMB) and ATM inhibition (ATMi), at steady state or after induction of
845 DNA damage by ETO for 30 min. Data represent the mean ± s.e.m.
846
847 **Fig. 6. Spatial dysregulation of RAD51C by depletion of Giantin leads to genomic**
848 **instability, inhibition of DDR signalling and accelerated cell proliferation.** (**A** and **B**)
849 Representative images and quantification of cells displaying micronuclei after siRNA
850 treatment; white arrows denote micronuclei structures. Data represent the mean ± s.e.m.
851 ($n = 3$ biologically independent samples with over 10,000 cell analysed). (**C**) Representative
852 images of comet assay detection genomic DNA fragmentation in HK cells treated with
853 control, Giantin, or RAD51C targeting siRNA. (**D**) Quantification of comet OliveMoment. Data
854 represent the mean ± s.e.m. ($n = 3$ biologically independent samples). (**E** to **H**)
855 Representative images of colony formation ability for (**E**) HK and (**G**) U-2 OS cell lines.
856 Quantitative analysis of colony area coverage for (**F**) HK and (**G**) U-2 OS cell lines. Statistical
857 significance was determined using a two-tailed unpaired Student's t-test. Scale bars, 10 μm.
858 (**I** and **J**) WB analysis showing HK cells transfected with control, Giantin and GMAP210
859 siRNA and treated with DOX (40 μM) for 3 h. after 72 h transfection, the extracts were
860 prepared and immunoblotted as indicated ($n = 2$ biologically independent samples). (**K**) WB
861 showing HK cell extracts treated with DOX (40 μM) and IPZ (20 μM) for 3h. (**L**) WB analysis

862 showing HK cells transfected with siRNAs against Giantin, RAD51C or a combination of
863 Giantin and RAD51C for 72 h; and treated with DMSO, DOX (40 μM; 3h) or ETO (10 μM; 3
864 h). (**M**) Quantification of WB analysis showing the relative levels of pATM; (n=3 biological
865 independent experiments), data represent the mean ± s.e.m. Quantification of (**N**) cells
866 displaying micronuclei and (**O**) fold change in cell number after siRNA treatment (n=3
867 biological independent experiments with at least 1000 cells analysed per condition), data
868 represent the mean ± s.e.m. (**P**) Proposed model for the regulation of HR-mediated repair at
869 the Golgi complex. In response to double-strand DNA breaks, DDR is activated at the
870 nucleus, ATM signal transduction from the nucleus to the Golgi leads to the phosphorylation
871 of the Golgi population of NBN, anchored by GMAP210. This leads to the dissociation of
872 RAD51C which is anchored to the Golgi through its interaction with the cytoplasmic tail of
873 Giantin, this RAD51C Golgi population redistributes to form nuclear foci. This transport step
874 requires Importin-beta-mediated nuclear import. The spatiotemporal regulation of RAD51C
875 is required for the correct activation of HR DNA repair and the regulation of DDR response.
876
877 **fig. S1.** Representative images of HK cells stained with antibodies against DDR proteins and
878 the Golgi marker, GM130. Cells were treated with a control or an siRNA against the protein
879 of interest to validate the specificity of the antibody. The changes in intensity measurements
880 in the Golgi and nuclear compartment were quantified (n=2, biological independent samples
881 with at least 500 cells analysed for each treatment). Scale bar, 10 μm. Continued on **fig.**
882 **S2A**.
883
884 **fig. S2**. (**A**) Representative images of HK cells stained with antibodies against DDR proteins
885 and the Golgi marker, GM130. Cells were treated with a control or an siRNA against the
886 protein of interest to validate the specificity of the antibody. The changes in intensity
887 measurements in the Golgi and nuclear compartment were quantified. (n=2, biological
888 independent samples with at least 500 cells analysed for each treatment). (**B**)
889 Experimentally-based protein-protein interaction networks displaying the Golgi-nuclear
890 localisation proteins validated in this study. Proteins are categorised by functional pathways
891 annotated using gene ontology terms (**Supplementary Table S1**).
892
893 **fig. S3**. (**A**) Representative images of HK cells were stained with antibodies against DDR
894 proteins and the Golgi marker, GM130. HK cells were treated with DOX (40 μM, 3 h), fixed
895 and stained with antibodies against DDR proteins and the Golgi marker, GM130 (**A** to **C**);
896 yellow arrows denote the Golgi membranes. Scale bar, 10 μm. Quantification of the relative
897 intensity of DDR proteins at the Golgi (**B**) and the nucleus (**C**) DOX treated normalised to
898 untreated control. Data represent the mean ± s.e.m. ($n = 3$ biologically independent samples
899 with at least 200 cells analysed for each protein in control and treatment conditions). The
900 proteins are classified according to their Golgi localisation patterns (**Fig. 2E**). Statistical
901 significance was determined using a two-tailed unpaired Student's *t*-test; ns $P > 0.05$, $^{**}P <$
902 0.01, $^{***}P < 0.001$, $^{****}P < 0.0001$, compared to untreated control. (**D**) Golgi-cisternal
903 localisation analysis of Golgi-nuclear DDR proteins. HK cells were treated with Nocodazole
904 (33 μM, 3 h), fixed and stained with antibodies against DDR proteins. Quantification of
905 Pearson's correlation coefficient (PCC) between *cis*-Golgi and *trans*-Golgi markers and DDR
906 proteins; N ≥ 4 cells; n ≥ 36 mini stacks.
907
908 **fig. S4**. (**A**) Representative images of HK cells were stained with antibodies against DDR
909 proteins and the Golgi marker, GM130. HK cells were treated with H_2O_2 (50 μM, for 20 min

910 followed by 15 min recovery), fixed and stained with antibodies against DDR proteins and
911 the Golgi marker, GM130 (**A** to **C**); yellow arrows denote the Golgi membranes. Scale bar,
912 10 µm. Quantification of the relative intensity of DDR proteins at the Golgi (**B**) and the nucleus
913 (**C**) H_2O_2 treated normalised to untreated control. Data represent the mean ± s.e.m. (*n* = 3
914 biologically independent samples with at least 200 cells analysed for each protein in control
915 and treatment conditions). The proteins are classified according to their Golgi localisation
916 patterns (**Fig. 2E**). Statistical significance was determined using a two-tailed unpaired
917 Student's *t*-test; ns P > 0.05, **P < 0.01, ***P < 0.001, ****P <0.0001, compared to untreated
918 control.
919
920 **fig. S5**. (**A**) Representative images of HK cells were stained with antibodies against DDR
921 proteins and the Golgi marker, GM130. HK cells were treated with $KBrO_3$ (5 mM, 3h), fixed
922 and stained with antibodies against DDR proteins and the Golgi marker, GM130 (A to D);
923 yellow arrows denote the Golgi membranes. Scale bar, 10 µm. (**B**) A ratio of DDR protein
924 Golgi-nuclear distribution after treatment with $KBrO_3$. Quantification of the relative intensity
925 of DDR proteins at the Golgi (**C**) and the nucleus (d) $KBrO_3$ treated normalised to untreated
926 control. Data represent the mean ± s.e.m. (*n* = 3 biologically independent samples with at
927 least 200 cells analysed for each protein in control and treatment conditions). The proteins
928 are classified according to their Golgi localisation patterns (**Fig. 2E**). Statistical significance
929 was determined using a two-tailed unpaired Student's *t*-test; ns P > 0.05, **P < 0.01, ***P <
930 0.001, ****P <0.0001, compared to untreated control.
931
932 **fig. S6**. (**A**) Representative images showing the RAD51C antibody specificity. HK cells were
933 stained with antibodies against RAD51C and GM130; DNA was stained with Hoechst 33342.
934 (**B**) Quantification of RAD51C sum intensity after RAD51C depletion. Data represent the
935 mean ± s.e.m. (n = 3 biologically independent samples with a total of 831 cells analysed). (**C**)
936 Western blot analysis showing the level of RAD51C protein level, in RAD51C-depleted and
937 control cells (n = 3 biologically independent samples). Statistical significance was determined
938 using a two-tailed unpaired Student's t-test. (**D**) Western blot showing the subcellular
939 localisation of RAD51C treated with the DMSO and doxorubicin. The protein levels
940 normalised against the respective fraction control ($RAD51C^{mem}$/GM130; $RAD51C^{nuc}$/Lamin
941 B1; $RAD51C^{cyt}$/tubulin). Data represent the mean ± s.e.m; (n = 2 biologically independent
942 samples). (**E**) Quantification of RAD51C membrane-nuclear distribution ratio after treatment
943 with DOX, calculated from isolated fractions.
944
945 **fig. S7**. Representative images of HK cells were stained with antibodies against RAD51C
946 and GM130. (**A**) Cells were treated with DMSO or IPZ prior to a 3-hour treatment with DOX.
947 (**B**) HK cells were treated with DMSO (control) alone or with ATM inhibitor (KU55933), ATR
948 inhibitor (VE-821) or DNA-PK inhibitor (NU7441) prior to a 3-hour treatment with doxorubicin.
949 Yellow arrows denote the Golgi membrane; white denotes nuclear foci. Scale bars, 10 µm.
950
951 **fig. S8**. HK cells stained with antibodies against RAD51C and GM130. Cells were treated
952 with (**A**) Camptothecin (CPT), (**D**) etoposide (ETO) and (**G**) mitomycin C (MMC) for 16 h
953 followed by media change for 2 h; scale bar 10 µm. Quantification of RAD51C distribution
954 between the Golgi and nuclear compartment after (**B**) CPT, (**E**) ETO and (**H**) MMC
955 treatments. Quantification of RAD51C distribution between the Golgi and nuclear
956 compartment after (**C**) CPT, (**F**) ETO and (**I**) MMC treatments. Data represent the
957 mean ± s.e.m. (*n* = 3 biologically independent samples with more than 600 cells analysed per

958 treatment). Statistical significance was determined using a two-tailed unpaired Student's *t*-
959 test. **P<0.01; ***P<0.001.
960
961 **fig. S9.** (**A**) siRNA screen data (*32*) showing the relative Homologous Recombination (HR)
962 repair rate upon systematic knockdown of the Golgin protein family (grey) and HR complex
963 proteins (black). (**B**) siRNA screen data (*31*) showing the relative percent cell population with
964 phosphorylation of H2AX upon systematic knockdown of the Golgins. The datasets are
965 normalised to the negative control set at 1. (**C**) HK cells were transfected with control, or
966 Giantin siRNAs for 72 hours. The cells were stained with antibodies against Giantin and
967 nuclei were stained with Hoechst 33342; scale bar 10 µm. (**D**) HK cells stained with
968 antibodies against pNBN (s343) and GM130. Various treatments were applied to the cells:
969 GMAP210 knockdown, ATM inhibitors, and leptomycin B (LMB) to block nuclear export.
970 These treatments were conducted under both control conditions and following a 30-minute
971 induction of DNA damage using etoposide. (**E**) Cell cycle profile of HK cell treated with
972 Giantin or control siRNA. Data represent the mean ± s.e.m. ($n = 3$ biologically independent
973 samples). (**F** and **G**) Kaplan-Meier survival plots in patients with high and low mRNA (f) (*57*)
974 and protein (**G**) (*58*) Giantin expression in Breast Cancer patients. The graph was generated
975 using the kmplot database (https://kmplot.com).
976
977 **fig. S10.** Western blot analysis showing the level of proteins in siRNA-depleted and control
978 cells for the validation of antibody specificity for (**A**) ATM and (**B**) NBN. The changes in
979 protein level were quantified as relative protein level normalised to alpha-tubulin.
980
981 **Supplementary Table S1.** Set of tables listing the antibodies and siRNA used for the
982 analysis of Human Protein Atlas dataset for the identification and validation of dual-localising
983 Golgi-nuclear proteins. Table 1 presents the antibodies and siRNA used; Table 2 presents
984 the identified and validated Golgi-nuclear protein. Table 3 presents the gene ontology and
985 enrichment terms of the validated Golgi-nuclear proteins.
986
987 **Supplementary Table S2.** Table listing the cross-correlation measure for analysis of Golgi
988 cisternal localisation analysis of dual-localising DDR proteins.
989
990 **References:**
991

992 1. C. Wilson, R. Venditti, L. R. Rega, A. Colanzi, G. D'Angelo, M. A. De Matteis, The Golgi
993 apparatus: an organelle with multiple complex functions. *Biochem. J* **433**, 1–9 (2011).
994 2. C. Makhoul, P. Gosavi, P. A. Gleeson, The Golgi architecture and cell sensing. *Biochem.*
995 *Soc. Trans.* **46**, 1063–1072 (2018).
996 3. H. H. Freeze, B. G. Ng, Golgi glycosylation and human inherited diseases. *Cold Spring*
997 *Harb. Perspect. Biol.* **3**, a005371 (2011).
998 4. C. E. Machamer, The Golgi complex in stress and death. *Front. Neurosci.* **9**, 421 (2015).
999 5. F. Zappa, M. Failli, M. A. De Matteis, The Golgi complex in disease and therapy. *Curr.*
1000 *Opin. Cell Biol.* **50**, 102–116 (2018).
1001 6. J. Liu, Y. Huang, T. Li, Z. Jiang, L. Zeng, Z. Hu, The role of the Golgi apparatus in
1002 disease (Review). *Int. J. Mol. Med.* **47** (2021).
1003 7. K. Haze, H. Yoshida, H. Yanagi, T. Yura, K. Mori, Mammalian transcription factor ATF6
1004 is synthesized as a transmembrane protein and activated by proteolysis in response to
1005 endoplasmic reticulum stress. *Mol. Biol. Cell* **10**, 3787–3799 (1999).
1006 8. M. S. Brown, A. Radhakrishnan, J. L. Goldstein, Retrospective on Cholesterol
1007 Homeostasis: The Central Role of Scap. *Annu. Rev. Biochem.* **87**, 783–807 (2018).

9. A. Petrosyan, Onco-Golgi: Is Fragmentation a Gate to Cancer Progression? *Biochem Mol Biol J* **1** (2015).
10. P. Kulkarni-Gosavi, C. Makhoul, P. A. Gleeson, Form and function of the Golgi apparatus: scaffolds, cytoskeleton and signalling. *FEBS Lett.* **593**, 2289–2305 (2019).
11. X. Zhang, Alterations of Golgi Structural Proteins and Glycosylation Defects in Cancer. *Front Cell Dev Biol* **9**, 665289 (2021).
12. S. E. Farber-Katz, H. C. Dippold, M. D. Buschman, M. C. Peterman, M. Xing, C. J. Noakes, J. Tat, M. M. Ng, J. Rahajeng, D. M. Cowan, G. J. Fuchs, H. Zhou, S. J. Field, DNA damage triggers Golgi dispersal via DNA-PK and GOLPH3. *Cell* **156**, 413–427 (2014).
13. S. Bui, I. Mejia, B. Díaz, Y. Wang, Adaptation of the Golgi Apparatus in Cancer Cell Invasion and Metastasis. *Front Cell Dev Biol* **9**, 806482 (2021).
14. P. J. Thul, L. Åkesson, M. Wiking, D. Mahdessian, A. Geladaki, H. Ait Blal, T. Alm, A. Asplund, L. Björk, L. M. Breckels, A. Bäckström, F. Danielsson, L. Fagerberg, J. Fall, L. Gatto, C. Gnann, S. Hober, M. Hjelmare, F. Johansson, S. Lee, C. Lindskog, J. Mulder, C. M. Mulvey, P. Nilsson, P. Oksvold, J. Rockberg, R. Schutten, J. M. Schwenk, Å. Sivertsson, E. Sjöstedt, M. Skogs, C. Stadler, D. P. Sullivan, H. Tegel, C. Winsnes, C. Zhang, M. Zwahlen, A. Mardinoglu, F. Pontén, K. von Feilitzen, K. S. Lilley, M. Uhlén, E. Lundberg, A subcellular map of the human proteome. *Science* **356** (2017).
15. C. Stadler, M. Hjelmare, B. Neumann, K. Jonasson, R. Pepperkok, M. Uhlén, E. Lundberg, Systematic validation of antibody binding and protein subcellular localization using siRNA and confocal microscopy. *J. Proteomics* **75**, 2236–2251 (2012).
16. S. Y. Dejgaard, A. Murshid, K. M. Dee, J. F. Presley, Confocal microscopy-based linescan methodologies for intra-Golgi localization of proteins. *J. Histochem. Cytochem.* **55**, 709–719 (2007).
17. C. F. Thorn, C. Oshiro, S. Marsh, T. Hernandez-Boussard, H. McLeod, T. E. Klein, R. B. Altman, Doxorubicin pathways: pharmacodynamics and adverse effects. *Pharmacogenet. Genomics* **21**, 440–446 (2011).
18. E. S. Henle, S. Linn, Formation, prevention, and repair of DNA damage by iron/hydrogen peroxide. *J. Biol. Chem.* **272**, 19095–19098 (1997).
19. S. Loft, X. S. Deng, J. Tuo, A. Wellejus, M. Sørensen, H. E. Poulsen, Experimental study of oxidative DNA damage. *Free Radic. Res.* **29**, 525–539 (1998).
20. S. Badie, C. Liao, M. Thanasoula, P. Barber, M. A. Hill, M. Tarsounas, RAD51C facilitates checkpoint signaling by promoting CHK2 phosphorylation. *J. Cell Biol.* **185**, 587–600 (2009).
21. R. Prakash, Y. Rawal, M. R. Sullivan, M. K. Grundy, H. Bret, M. J. Mihalevic, H. L. Rein, J. M. Baird, K. Darrah, F. Zhang, R. Wang, T. A. Traina, M. R. Radke, S. H. Kaufmann, E. M. Swisher, R. Guérois, M. Modesti, P. Sung, M. Jasin, K. A. Bernstein, Homologous recombination-deficient mutation cluster in tumor suppressor RAD51C identified by comprehensive analysis of cancer variants. *Proc. Natl. Acad. Sci. U. S. A.* **119**, e2202727119 (2022).
22. Y. Rawal, L. Jia, A. Meir, S. Zhou, H. Kaur, E. A. Ruben, Y. Kwon, K. A. Bernstein, M. Jasin, A. B. Taylor, S. Burma, R. Hromas, A. V. Mazin, W. Zhao, D. Zhou, E. V. Wasmuth, E. C. Greene, P. Sung, S. K. Olsen, Structural insights into BCDX2 complex function in homologous recombination. *Nature* **619**, 640–649 (2023).
23. L. A. Greenhough, C.-C. Liang, O. Belan, S. Kunzelmann, S. Maslen, M. C. Rodrigo-Brenni, R. Anand, M. Skehel, S. J. Boulton, S. C. West, Structure and function of the RAD51B-RAD51C-RAD51D-XRCC2 tumour suppressor. *Nature* **619**, 650–657 (2023).
24. K. A. Miller, J. M. Hinz, N. A. Yamada, L. H. Thompson, J. S. Albala, Nuclear localization of Rad51B is independent of Rad51C and BRCA2. *Mutagenesis* **20**, 57–63 (2005).
25. J. F. Soderholm, S. L. Bird, P. Kalab, Y. Sampathkumar, K. Hasegawa, M. Uehara-Bingen, K. Weis, R. Heald, Importazole, a small molecule inhibitor of the transport receptor importin-β. *ACS Chem. Biol.* **6**, 700–708 (2011).
26. A. Ciccia, S. J. Elledge, The DNA damage response: making it safe to play with knives. *Mol. Cell* **40**, 179–204 (2010).

1063 27. I. Hickson, Y. Zhao, C. J. Richardson, S. J. Green, N. M. B. Martin, A. I. Orr, P. M.
1064 Reaper, S. P. Jackson, N. J. Curtin, G. C. M. Smith, Identification and characterization
1065 of a novel and specific inhibitor of the ataxia-telangiectasia mutated kinase ATM. *Cancer*
1066 *Res.* **64**, 9152–9159 (2004).
1067 28. E. Fokas, R. Prevo, J. R. Pollard, P. M. Reaper, P. A. Charlton, B. Cornelissen, K. A.
1068 Vallis, E. M. Hammond, M. M. Olcina, W. Gillies McKenna, R. J. Muschel, T. B. Brunner,
1069 Targeting ATR in vivo using the novel inhibitor VE-822 results in selective sensitization
1070 of pancreatic tumors to radiation. *Cell Death Dis.* **3**, e441 (2012).
1071 29. M. Tavecchio, J. M. Munck, C. Cano, D. R. Newell, N. J. Curtin, Further characterisation
1072 of the cellular activity of the DNA-PK inhibitor, NU7441, reveals potential cross-talk with
1073 homologous recombination. *Cancer Chemother. Pharmacol.* **69**, 155–164 (2012).
1074 30. C. Jekimovs, E. Bolderson, A. Suraweera, M. Adams, K. J. O'Byrne, D. J. Richard,
1075 Chemotherapeutic compounds targeting the DNA double-strand break repair pathways:
1076 the good, the bad, and the promising. *Front. Oncol.* **4**, 86 (2014).
1077 31. R. D. Paulsen, *A Genome-Wide SiRNA Screen Reveals Diverse Cellular Processes and*
1078 *Pathways That Mediate Genomic Stability* (Stanford University, 2010).
1079 32. B. Adamson, A. Smogorzewska, F. D. Sigoillot, R. W. King, S. J. Elledge, A genome-
1080 wide homologous recombination screen identifies the RNA-binding protein RBMX as a
1081 component of the DNA-damage response. *Nat. Cell Biol.* **14**, 318–328 (2012).
1082 33. T. M. Witkos, M. Lowe, The Golgin Family of Coiled-Coil Tethering Proteins. *Front Cell*
1083 *Dev Biol* **3**, 86 (2015).
1084 34. A. C. Vítor, P. Huertas, G. Legube, S. F. de Almeida, Studying DNA Double-Strand
1085 Break Repair: An Ever-Growing Toolbox. *Front Mol Biosci* **7**, 24 (2020).
1086 35. M. Shrivastav, L. P. De Haro, J. A. Nickoloff, Regulation of DNA double-strand break
1087 repair pathway choice. *Cell Res.* **18**, 134–147 (2008).
1088 36. Y. Zhang, J. Zhou, C. U. Lim, The role of NBS1 in DNA double strand break repair,
1089 telomere stability, and cell cycle checkpoint control. *Cell Res.* **16**, 45–54 (2006).
1090 37. N. Kudo, B. Wolff, T. Sekimoto, E. P. Schreiner, Y. Yoneda, M. Yanagida, S. Horinouchi,
1091 M. Yoshida, Leptomycin B inhibition of signal-mediated nuclear export by direct binding
1092 to CRM1. *Exp. Cell Res.* **242**, 540–547 (1998).
1093 38. K. Krupina, A. Goginashvili, D. W. Cleveland, Causes and consequences of micronuclei.
1094 *Curr. Opin. Cell Biol.* **70**, 91–99 (2021).
1095 39. P. Møller, The comet assay: ready for 30 more years. *Mutagenesis* **33**, 1–7 (2018).
1096 40. J. A. Rodriguez, S. Schüchner, W. W. Y. Au, M. Fabbro, B. R. Henderson, Nuclear-
1097 cytoplasmic shuttling of BARD1 contributes to its proapoptotic activity and is regulated
1098 by dimerization with BRCA1. *Oncogene* **23**, 1809–1820 (2004).
1099 41. Z. Feng, L. Kachnic, J. Zhang, S. N. Powell, F. Xia, DNA Damage Induces p53-
1100 dependent BRCA1 Nuclear Export*. *J. Biol. Chem.* **279**, 28574–28584 (2004).
1101 42. M. E. Thompson, BRCA1 16 years later: nuclear import and export processes. *FEBS J.*
1102 **277**, 3072–3078 (2010).
1103 43. J.-H. Wei, Z. C. Zhang, R. M. Wynn, J. Seemann, GM130 Regulates Golgi-Derived
1104 Spindle Assembly by Activating TPX2 and Capturing Microtubules. *Cell* **162**, 287–299
1105 (2015).
1106 44. C.-C. Chang, C.-J. Chen, C. Grauffel, Y.-C. Pien, C. Lim, S.-Y. Tsai, K.-C. Hsia, Ran
1107 pathway-independent regulation of mitotic Golgi disassembly by Importin-α. *Nat.*
1108 *Commun.* **10**, 4307 (2019).
1109 45. R. D. Paulsen, D. V. Soni, R. Wollman, A. T. Hahn, M.-C. Yee, A. Guan, J. A. Hesley,
1110 S. C. Miller, E. F. Cromwell, D. E. Solow-Cordero, T. Meyer, K. A. Cimprich, A genome-
1111 wide siRNA screen reveals diverse cellular processes and pathways that mediate
1112 genome stability. *Mol. Cell* **35**, 228–239 (2009).
1113 46. H. L. Rein, K. A. Bernstein, R. A. Baldock, RAD51 paralog function in replicative DNA
1114 damage and tolerance. *Curr. Opin. Genet. Dev.* **71**, 86–91 (2021).
1115 47. M. R. Sullivan, K. A. Bernstein, RAD-ical New Insights into RAD51 Regulation. *Genes*
1116 **9** (2018).
1117 48. K. Somyajit, S. Subramanya, G. Nagaraju, Distinct roles of FANCO/RAD51C protein in

DNA damage signaling and repair. *J. Biol. Chem.* **287**, 3366–3380 (2012).
49. K. Somyajit, S. Saxena, S. Babu, A. Mishra, G. Nagaraju, Mammalian RAD51 paralogs protect nascent DNA at stalled forks and mediate replication restart. *Nucleic Acids Res.* **43**, 9835–9855 (2015).
50. M. Berti, F. Teloni, S. Mijic, S. Ursich, J. Fuchs, M. D. Palumbieri, J. Krietsch, J. A. Schmid, E. B. Garcin, S. Gon, M. Modesti, M. Altmeyer, M. Lopes, Sequential role of RAD51 paralog complexes in replication fork remodeling and restart. *Nat. Commun.* **11**, 3531 (2020).
51. L. Wang, W. Wang, S. Zeng, H. Zheng, Q. Lu, Construction and validation of a 6-gene nomogram discriminating lung metastasis risk of breast cancer patients. *PLoS One* **15**, e0244693 (2020).
52. K. E. Craven, Y. Gökmen-Polar, S. S. Badve, CIBERSORT analysis of TCGA and METABRIC identifies subgroups with better outcomes in triple negative breast cancer. *Sci. Rep.* **11**, 4691 (2021).
53. A. Mathioudaki, V. Ljungström, M. Melin, M. L. Arendt, J. Nordin, Å. Karlsson, E. Murén, P. Saksena, J. R. S. Meadows, V. D. Marinescu, T. Sjöblom, K. Lindblad-Toh, Author Correction: Targeted sequencing reveals the somatic mutation landscape in a Swedish breast cancer cohort. *Sci. Rep.* **11**, 5310 (2021).
54. O. Pipek, D. Alpár, O. Rusz, C. Bödör, Z. Udvarnoki, A. Medgyes-Horváth, I. Csabai, Z. Szállási, L. Madaras, Z. Kahán, G. Cserni, B. Kővári, J. Kulka, A. M. Tőkés, Genomic Landscape of Normal and Breast Cancer Tissues in a Hungarian Pilot Cohort. *Int. J. Mol. Sci.* **24** (2023).
55. S. Ghannoum, D. Fantini, M. Zahoor, V. Reiterer, S. Phuyal, W. Leoncio Netto, Ø. Sørensen, A. Iyer, D. Sengupta, L. Prasmickaite, G. M. Mælandsmo, A. Köhn-Luque, H. Farhan, A combined experimental-computational approach uncovers a role for the Golgi matrix protein Giantin in breast cancer progression. *PLoS Comput. Biol.* **19**, e1010995 (2023).
56. J. Leighton, M. Hu, E. Sei, F. Meric-Bernstam, N. E. Navin, Reconstructing mutational lineages in breast cancer by multi-patient-targeted single-cell DNA sequencing. *Cell Genom* **3**, 100215 (2023).
57. B. Győrffy, Survival analysis across the entire transcriptome identifies biomarkers with the highest prognostic power in breast cancer. *Comput. Struct. Biotechnol. J.* **19**, 4101–4109 (2021).
58. Á. Ősz, A. Lánczky, B. Győrffy, Survival analysis in breast cancer using proteomic data from four independent datasets. *Sci. Rep.* **11**, 16787 (2021).
59. F. Baschieri, E. Uetz-von Allmen, D. F. Legler, H. Farhan, Loss of GM130 in breast cancer cells and its effects on cell migration, invasion and polarity. *Cell Cycle* **14**, 1139–1147 (2015).
60. G. Bhat, V.-R. Hothpet, M.-F. Lin, P.-W. Cheng, Shifted Golgi targeting of glycosyltransferases and α-mannosidase IA from giantin to GM130-GRASP65 results in formation of high mannose N-glycans in aggressive prostate cancer cells. *Biochimica et Biophysica Acta (BBA) - General Subjects* **1861**, 2891–2901 (2017).
61. H. Erfle, B. Neumann, P. Rogers, J. Bulkescher, J. Ellenberg, R. Pepperkok, Work flow for multiplexing siRNA assays by solid-phase reverse transfection in multiwell plates. *J. Biomol. Screen.* **13**, 575–580 (2008).
62. A. E. Carpenter, T. R. Jones, M. R. Lamprecht, C. Clarke, I. H. Kang, O. Friman, D. A. Guertin, J. H. Chang, R. A. Lindquist, J. Moffat, P. Golland, D. M. Sabatini, CellProfiler: image analysis software for identifying and quantifying cell phenotypes. *Genome Biol.* **7**, R100 (2006).
63. J. Schindelin, I. Arganda-Carreras, E. Frise, V. Kaynig, M. Longair, T. Pietzsch, S. Preibisch, C. Rueden, S. Saalfeld, B. Schmid, J.-Y. Tinevez, D. J. White, V. Hartenstein, K. Eliceiri, P. Tomancak, A. Cardona, Fiji: an open-source platform for biological-image analysis. *Nat. Methods* **9**, 676–682 (2012).
64. S. Vodenkova, A. Azqueta, A. Collins, M. Dusinska, I. Gaivão, P. Møller, A. Opattova, P. Vodicka, R. W. L. Godschalk, S. A. S. Langie, An optimized comet-based in vitro DNA

1173 repair assay to assess base and nucleotide excision repair activity. *Nat. Protoc.* **15**,
1174 3844–3878 (2020).
1175 65. B. M. Gyori, G. Venkatachalam, P. S. Thiagarajan, D. Hsu, M.-V. Clement, OpenComet:
1176 an automated tool for comet assay image analysis. *Redox Biol* **2**, 457–465 (2014).

FIGURE 1

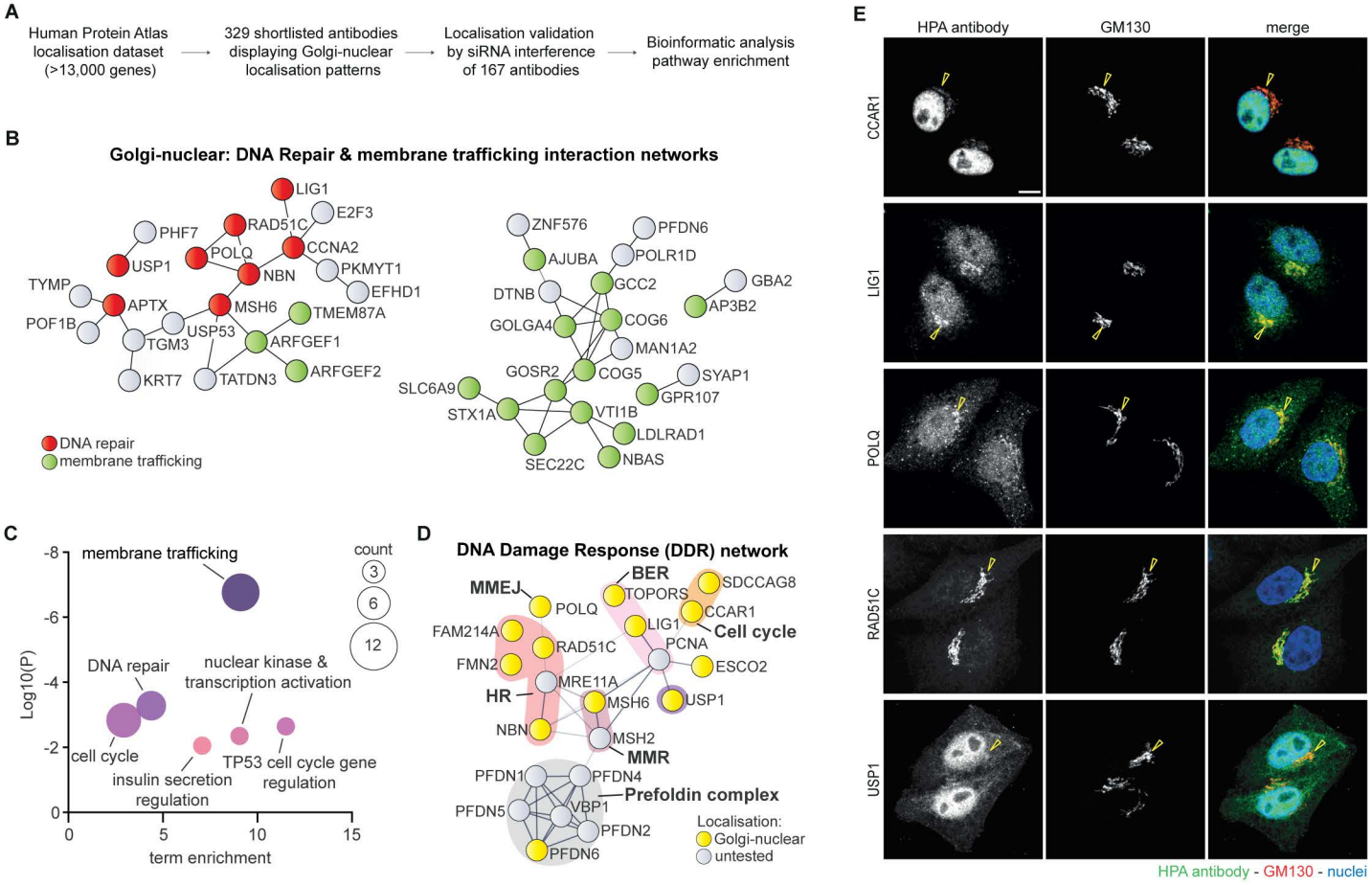

Fig. 1. Antibody-based analysis identifies a network of DNA damage response (DDR) proteins at the Golgi complex. (**A**) Schematic diagram of the screening process for the shortlisting, validation and characterisation of Golgi-nuclear localisation proteins, as a strategy to identify linking pathways. (**B**) Experimentally-based protein-protein interaction network displaying the DNA repair and membrane trafficking Golgi-nuclear localisation proteins validated in this study; categorised by functional pathways. (**C**) Pathway enrichment analysis of the Golgi-nuclear localisation proteins identified in this study. (**D**) Experimentally-based STRING protein-protein interaction network showing the DDR proteins identified to localise to both the Golgi complex and nucleus; yellow nodes indicate double-localising proteins, and grey nodes are filler untested proteins. (**E**) Representative images of HeLa Kyoto cells stained with antibodies against Golgi-nuclear DDR proteins (green), and the Golgi marker GM130 (red). DNA was stained with Hoechst 33342 (blue). Yellow arrowheads denote the Golgi complex. Scale bar, 10 µm.

FIGURE 2

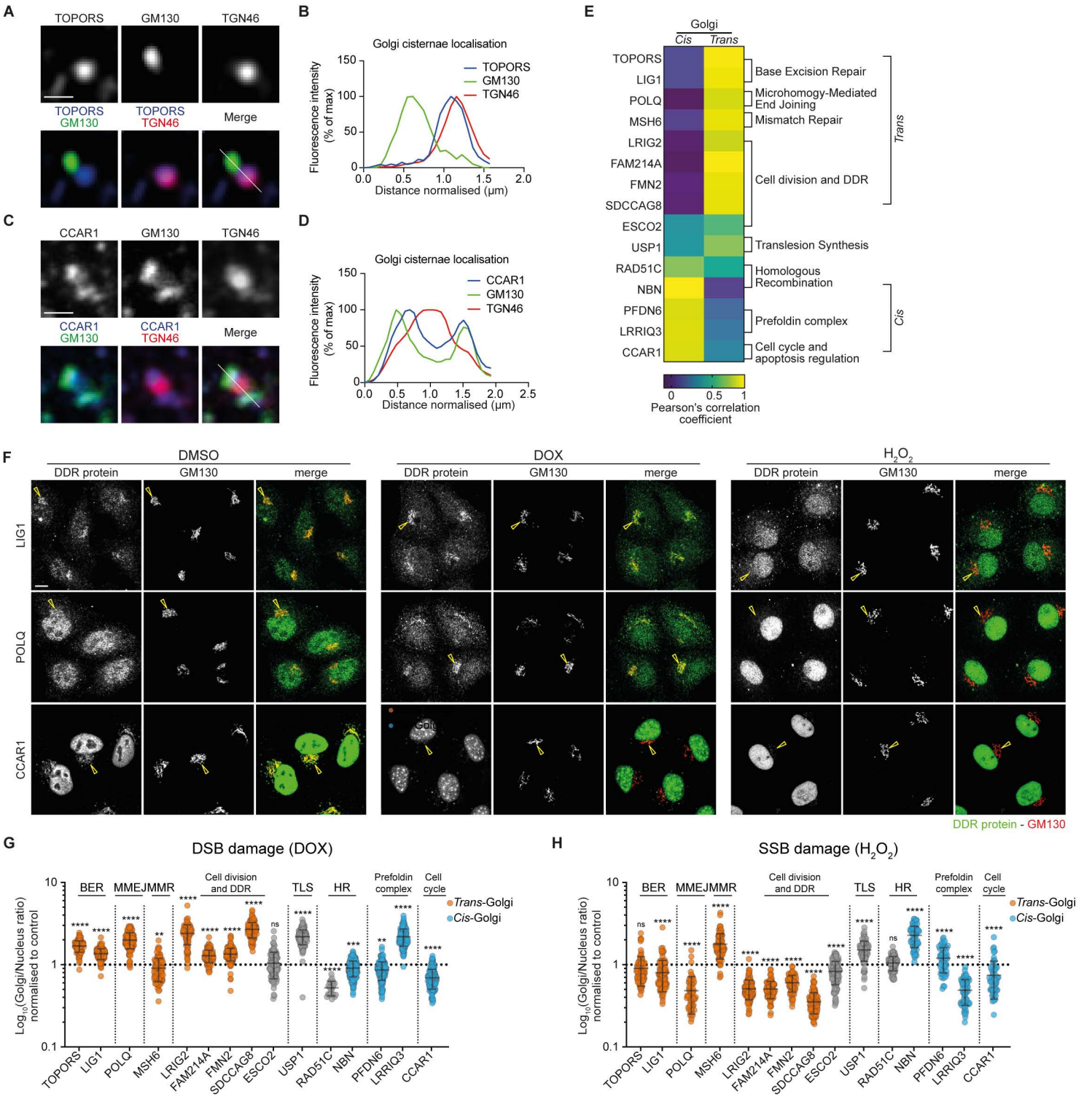

Fig. 2. Systematic analysis of Golgi-nuclear localisation DDR proteins. (**A** to **E**) Golgi-cisternal localisation analysis of Golgi-nuclear DDR proteins. HK cells were treated with Nocodazole (33 µM, 3 h), fixed and stained with antibodies against DDR proteins. (**A** and **C**) Enlarged view of single isolated mini-stack, where cells were stained with antibodies against TOPORS, CCAR1 and Golgi markers GM130 (*cis*-Golgi) and TGN46 (*trans*-Golgi); scale bar, 1 µm; (**B** and **D**) white lines across the stack depict the line-plot analysis. (**E**) Quantification of Pearson's correlation coefficient (PCC) between *cis*-Golgi and *trans*-Golgi markers and DDR proteins; n ≥ 36 mini-stacks. (**F**) Localisation changes of dual-localising DDR proteins upon induction of DNA damage. HK cells were treated with the DNA damage-inducing drug, doxorubicin (DOX) (40 µM, 3 h) or oxidative stress-inducing agent hydrogen peroxide (H_2O_2) (50 µM for 20 min, followed with 15 min recovery), fixed and stained with antibodies against DDR proteins LIG1, POLQ, CCAR1 and the Golgi marker, GM130; yellow arrows denote the Golgi membranes. Scale bars, 10 µm. (**G**) A ratio of DDR protein Golgi-nuclear distribution after treatment with DOX and (**H**) H_2O_2. Data represent the mean ± standard error of the mean (s.e.m.) (n = 3 biologically independent samples with at least 200 cells analysed for each protein in control and treatment conditions). The proteins are classified according to their Golgi localisation patterns (**E**). Statistical significance was determined using a two-tailed unpaired Student's t-test; ns P > 0.05, **P < 0.01, ***P < 0.001, ****P <0.0001, compared to untreated control.

FIGURE 3

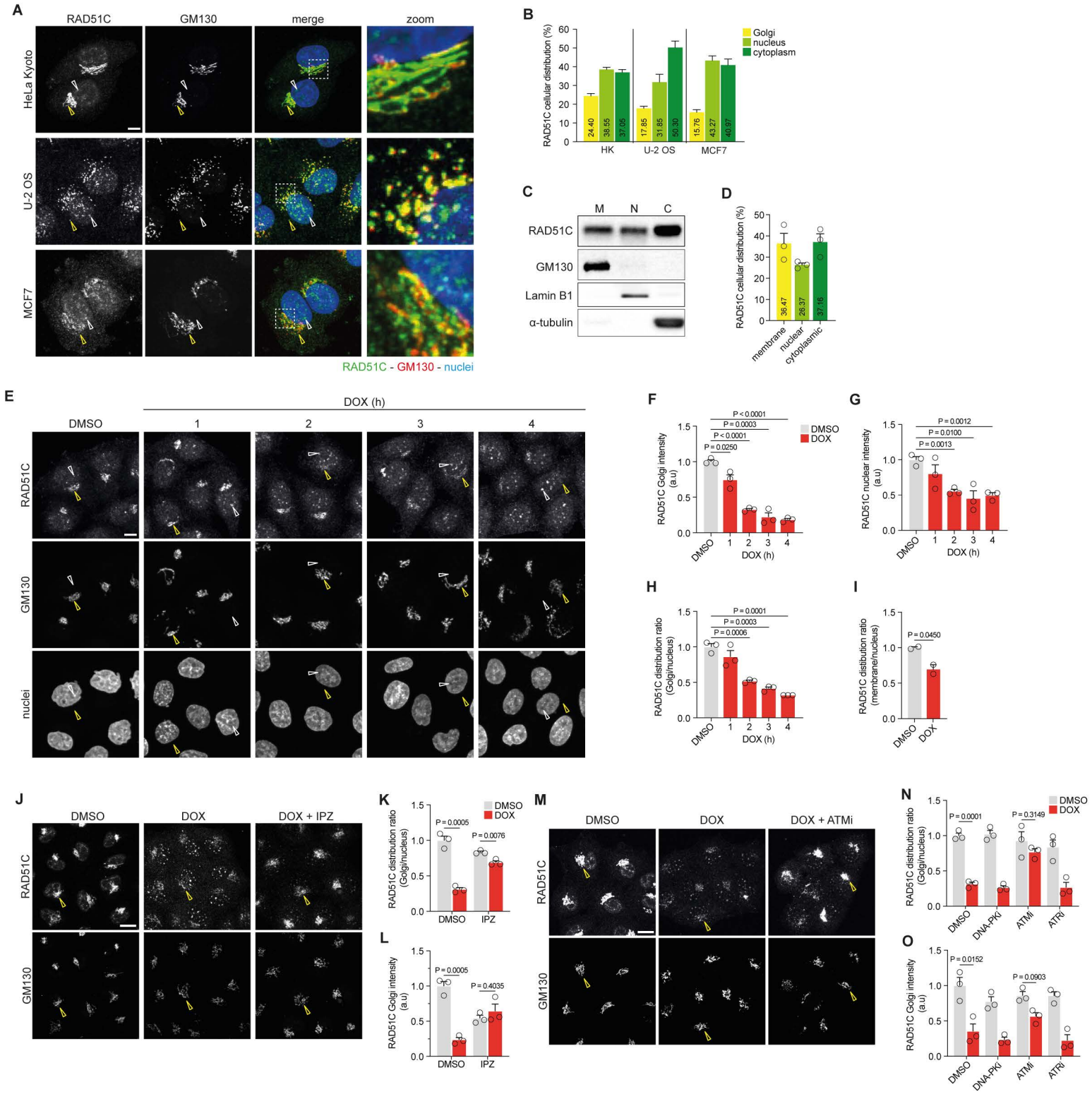

Fig. 3. Redistribution of RAD51C Golgi fraction is required for the formation of RAD51C nuclear foci and is dependent on the kinase ATM. (**A**) Representative images of HK, U-2 OS and MCF7 cells stained with antibodies against RAD51C (green) and GM130 (red). DNA stained with Hoechst 33342 (blue). (**B**) Quantification of RAD51C distribution across the Golgi, nucleus and cytoplasm in various cell lines quantified from immunofluorescence images. (**C**) WB analysis showing the subcellular membrane (M), nuclear (N) and cytoplasmic (C) fractions of RAD51C (markers: GM130 for Golgi membranes, Lamin B1 for the nuclear compartment, alpha-tubulin for the cytoplasmic fraction). (**D**) Quantification of western blot analysis showing the distribution of RAD51C in 3 cell fractions: membrane, nuclear and cytoplasmic; (n = 3 biologically independent experiments) data represent the mean ± s.e.m. (**E**) HK cells treated with the DNA damage-inducing drug, doxorubicin (DOX), for increasing lengths of time. Yellow arrows denote the Golgi membrane; white arrows denote nuclear foci. (**F**) Quantification of sum intensity of RAD51C Golgi population, (**G**) RAD51C nuclear population, and (**H**) a ratio of RAD51C Golgi-nuclear distribution after treatment with DOX. Data represent the s.e.m (n = 3 biologically independent samples with a total of 2343 cells analysed). (**I**) Quantification of RAD51C membrane-nuclear distribution ratio after treatment with DOX, calculated from isolated fractions (**fig. S6E**). HK cells were stained with antibodies against RAD51C and GM130. (**J**) Cells were treated with DMSO or IPZ prior to a 3-hour treatment with DOX. Yellow arrows denote the Golgi membrane; white denote nuclear foci. Results were quantified as (**K**) ratio of RAD51C Golgi-nuclear distribution and (**L**) relative sum intensity of RAD51C at the Golgi. Data represents s.e.m. (n = 3 biologically independent samples with a total of 445 cells analysed). (**M**) HK cells were treated with DMSO (control) alone or with ATM inhibitor (KU55933) or ATR inhibitor (VE-821) or DNA-PK inhibitor (NU7441) prior to a 3-hour treatment with doxorubicin. Results were quantified as (**N**) ratio of RAD51C Golgi-nuclear distribution and (**O**) relative sum intensity of RAD51C at the Golgi. Data represents s.e.m. (n = 3 biologically independent samples with a total of 1679 cells analysed). Scale bars, 10 μm. Statistical significance was determined using a two-tailed unpaired Student's t-test.

FIGURE 4

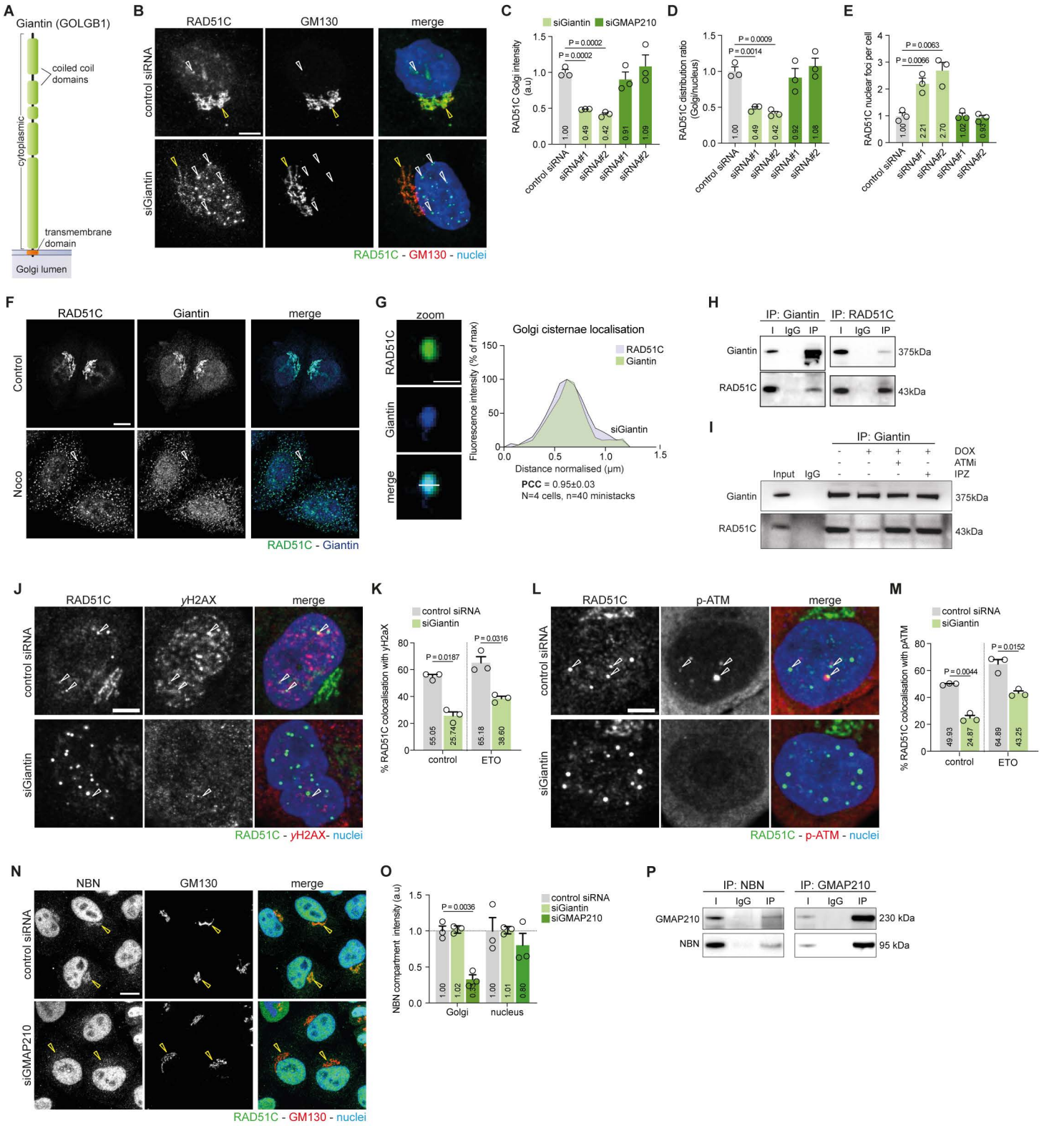

Fig. 4. RAD51C and NBN Golgi localisation is dependent on the Golgin proteins Giantin and GMAP210, respectively. (**A**) Graphical representation of Giantin protein configuration. (**B**) HK cells transfected with control or Giantin siRNAs for 72 hours, stained with antibodies against RAD51C and Golgi marker GM130. Yellow arrows indicate the Golgi and white arrows indicate nuclear foci. Quantification of the localisation changes of RAD51C quantified as (**C**) relative sum intensity of RAD51C at the Golgi, (**D**) fluorescent intensity ratio of the RAD51C Golgi-nuclear distribution and (**E**) relative number of RAD51C foci per cell. Data represent the mean ± s.e.m. (n = 3 biologically independent samples with a total of 1445 cells analysed). (**F**) Golgi-cisternal co-localisation analysis. HK cells treated with Nocodazole (33 µM, 3 h), fixed and stained with antibodies against Giantin and RAD51C. (**G**) Zoom enlarged view of single isolated mini-stack; scale bar, 1 µm; white line across the stack was used for line-scan analysis. (**H**) Immunoprecipitation of endogenous Giantin and RAD51C under control conditions and (**I**) after treatment with DOX or co-treatments ATMi and IPZ from HK cell extracts. (**J** to **M**) Co-localisation experiment of cells treated with control siRNA, or Giantin siRNA under control conditional or after treatment with ETO. Cells stained with antibody against RAD51C (green) and HR DDR markers (red): (**J**) y-H2AX, and (**L**) p-ATM. Co-localisation of structure is denoted by an arrowhead. Quantification of percentage RAD51C foci co-localising with (**K**) y-H2AX and (**M**) p-ATM. Data represent the mean ± s.e.m. (n = 3 biologically independent samples with at least 200 cells and at least 550 RAD51C nuclear foci analysed for the co-localisation experiments for each condition). (**N**) HK cells were transfected with control, Giantin or GMAP210 siRNAs for 72 hours and stained with antibodies against NBN and Golgi marker, GM130. Yellow arrows indicate the Golgi. (**O**) Quantification of the localisation changes of NBN were quantified as relative sum intensity of NBN at the Golgi and nucleus. (**P**) Co-immunoprecipitation of endogenous GMAP210 and NBN. Statistical significance was determined using a two-tailed unpaired Student's t-test. Scale bars, 10 µm.

FIGURE 5

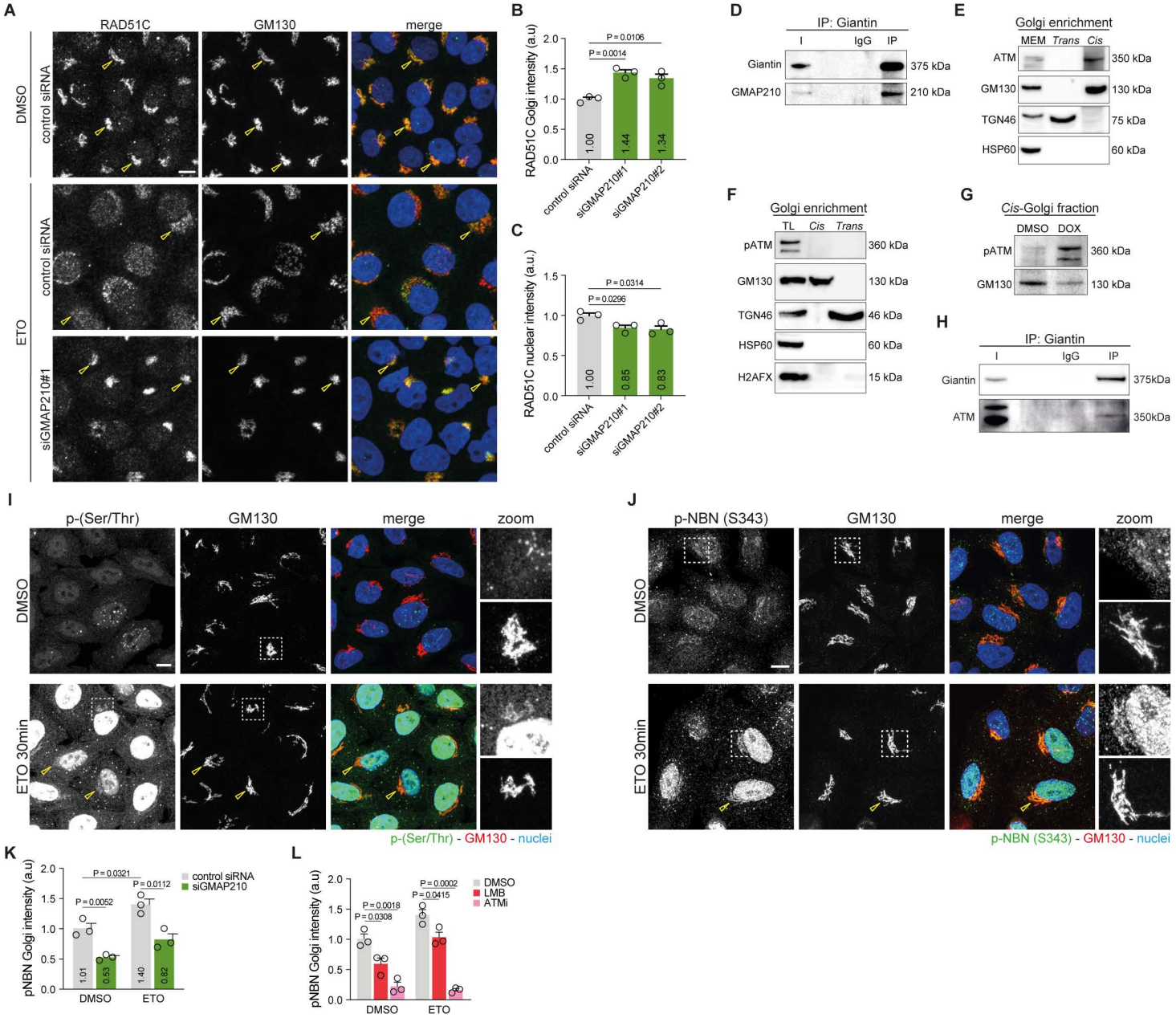

Fig. 5. GMAP210 is required for RAD51C nuclear redistribution in response to DSBs. (**A**) HK cells transfected with control or GMAP210 siRNAs and treated with solvent control DMSO or ETO (10 μM), stained with antibodies against RAD51C and Golgi marker, GM130. Yellow arrows indicate the Golgi. RAD51C redistribution changes after treatment with ETO were quantified for (**B**) the Golgi and (**C**) nuclear compartment. (**D**) Co-immunoprecipitation of endogenous Giantin with GMAP210 from HK cell extracts. (**E** to **G**) Western blot analysis of HK *cis*- and *trans*-Golgi enriched protein fractions, probing for (**E**) ATM, and (**F**) pATM under control conditions and (**G**) pATM after treatment with DOX (40 μ M) (markers: GM130 for *cis*-Golgi, TGN46 for *trans*-Golgi, HSP60 for mitochondria, H2AFX for nuclei). (**H**) Co-immunoprecipitation of endogenous Giantin with ATM from HK cell extract. (**I** and **J**) HK cells treated with solvent control, DMSO or ETO (10 μM) for 30 min. Cells stained with antibodies against GM130 and (**I**) phosphorylated SQ/TQ (pS/TQ) motifs, which recognise ATM/ATR substrates, the intensity of the image was intentionally increased, resulting in some structures being oversaturated. This was done to enhance the visibility of Golgi signal; (**J**) pNBN (S343). Yellow arrows indicate the Golgi. Quantification of the relative change in NBN phosphorylation level at the Golgi in response to (**K**) GMAP210 depletion, (**L**) nuclear export block by leptomycin B (LMB) and ATM inhibition (ATMi), at steady state or after induction of DNA damage by ETO for 30 min. Data represent the mean ± s.e.m.

FIGURE 6

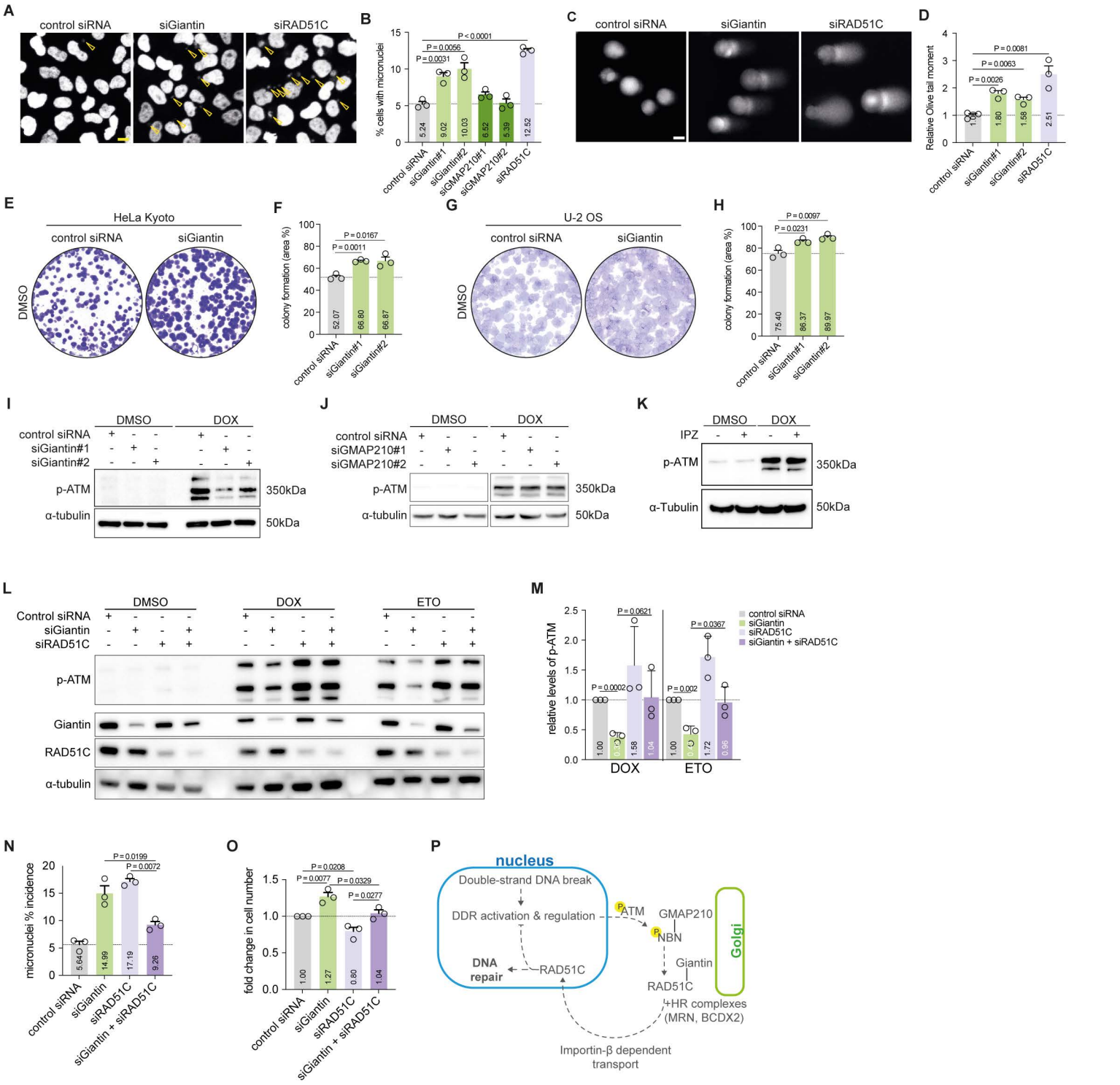

Fig. 6. Spatial dysregulation of RAD51C by depletion of Giantin leads to genomic instability, inhibition of DDR signalling and accelerated cell proliferation. (**A** and **B**) Representative images and quantification of cells displaying micronuclei after siRNA treatment; white arrows denote micronuclei structures. Data represent the mean ± s.e.m. (n = 3 biologically independent samples with over 10,000 cell analysed). (**C**) Representative images of comet assay detection genomic DNA fragmentation in HK cells treated with control, Giantin, or RAD51C targeting siRNA. (**D**) Quantification of comet OliveMoment. Data represent the mean ± s.e.m. (n = 3 biologically independent samples). (**E** to **H**) Representative images of colony formation ability for (**E**) HK and (**G**) U-2 OS cell lines. Quantitative analysis of colony area coverage for (**F**) HK and (**G**) U-2 OS cell lines. Statistical significance was determined using a two-tailed unpaired Student's t-test. Scale bars, 10 μm. (**I** and **J**) WB analysis showing HK cells transfected with control, Giantin and GMAP210 siRNA and treated with DOX (40 μM) for 3 h. after 72 h transfection, the extracts were prepared and immunoblotted as indicated (n = 2 biologically independent samples). (**K**) WB showing HK cell extracts treated with DOX (40 μM) and IPZ (20 μM) for 3h. (**L**) WB analysis showing HK cells transfected with siRNAs against Giantin, RAD51C or a combination of Giantin and RAD51C for 72 h; and treated with DMSO, DOX (40 μM; 3h) or ETO (10 μM; 3 h). **(M)** Quantification of WB analysis showing the relative levels of pATM; (n=3 biological independent experiments), data represent the mean ± s.e.m. Quantification of (**N**) cells displaying micronuclei and (**O**) fold change in cell number after siRNA treatment (n=3 biological independent experiments with at least 1000 cells analysed per condition), data represent the mean ± s.e.m. (**P**) Proposed model for the regulation of HR-mediated repair at the Golgi complex. In response to double-strand DNA breaks, DDR is activated at the nucleus, ATM signal transduction from the nucleus to the Golgi leads to the phosphorylation of the Golgi population of NBN, anchored by GMAP210. This leads to the dissociation of RAD51C which is anchored to the Golgi through its interaction with the cytoplasmic tail of Giantin, this RAD51C Golgi population redistributes to form nuclear foci. This transport step requires Importin-beta-mediated nuclear import. The spatiotemporal regulation of RAD51C is required for the correct activation of HR DNA repair and the regulation of DDR response.

SUPPLEMENTARY FIGURE 1

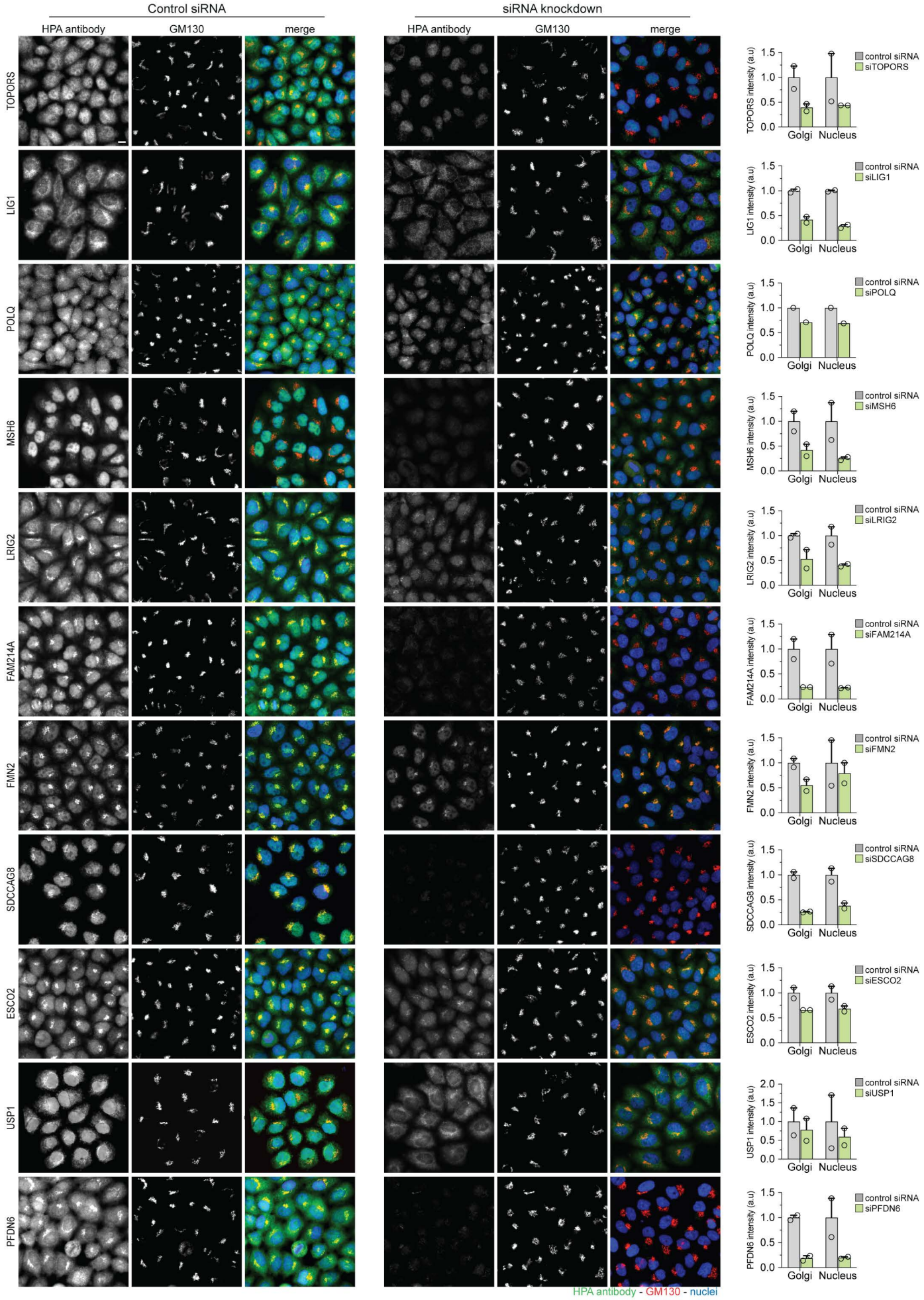

Fig. S1. Representative images of HK cells stained with antibodies against DDR proteins and the Golgi marker, GM130. Cells were treated with a control or an siRNA against the protein of interest to validate the specificity of the antibody. The changes in intensity measurements in the Golgi and nuclear compartment were quantified (n=2, biological independent samples with at least 500 cells analysed for each treatment). Scale bar, 10 µm. Continued on **Fig. S2A.**

SUPPLEMENTARY FIGURE 2

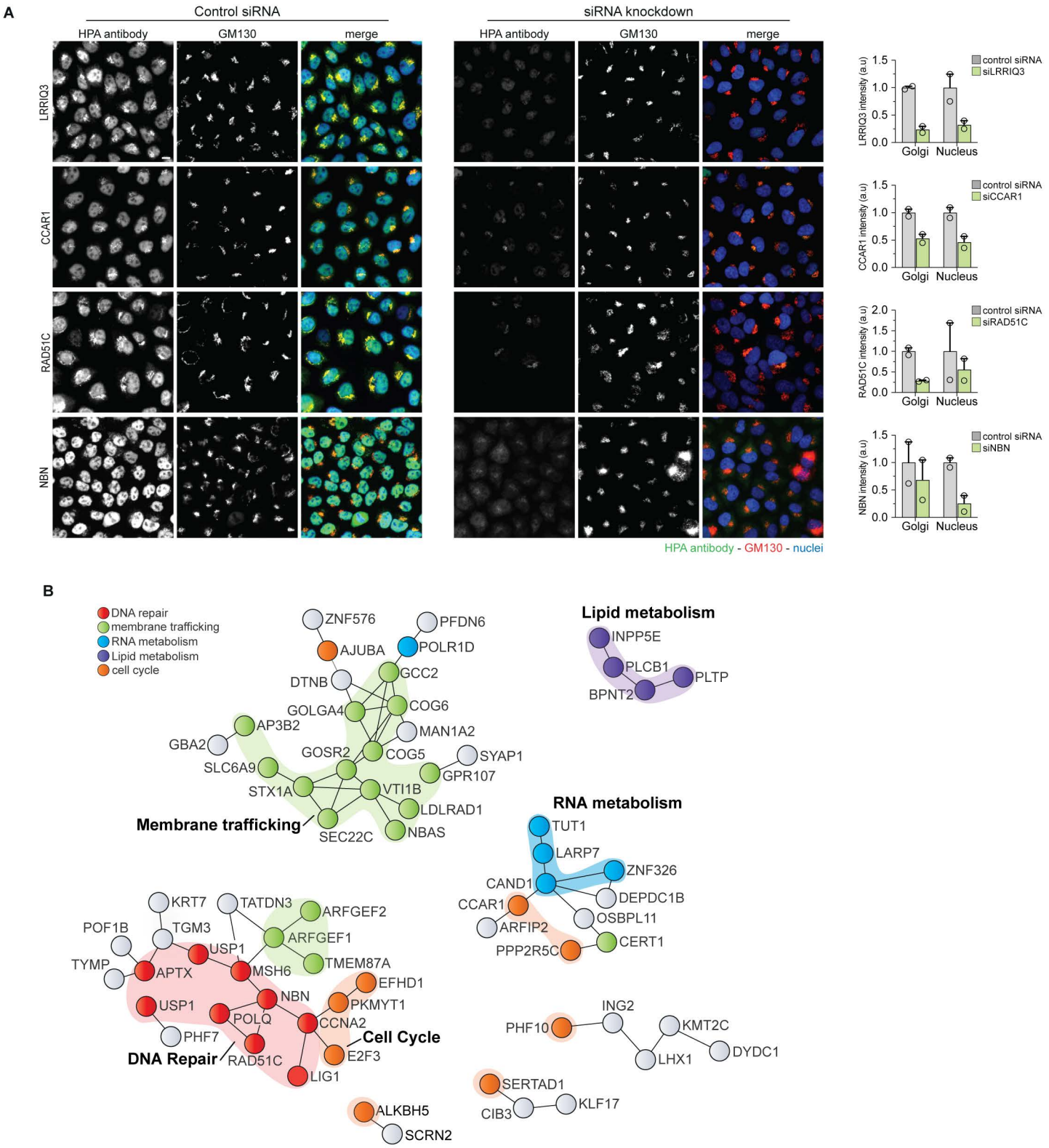

Fig. S2. (**A**) Representative images of HK cells stained with antibodies against DDR proteins and the Golgi marker, GM130. Cells were treated with a control or an siRNA against the protein of interest to validate the specificity of the antibody. The changes in intensity measurements in the Golgi and nuclear compartment were quantified. (n=2, biological independent samples with at least 500 cells analysed for each treatment). (**B**) Experimentally-based protein-protein interaction networks displaying the Golgi-nuclear localisation proteins validated in this study. Proteins are categorised by functional pathways annotated using gene ontology terms **(Supplementary Table S1)**.

SUPPLEMENTARY FIGURE 3

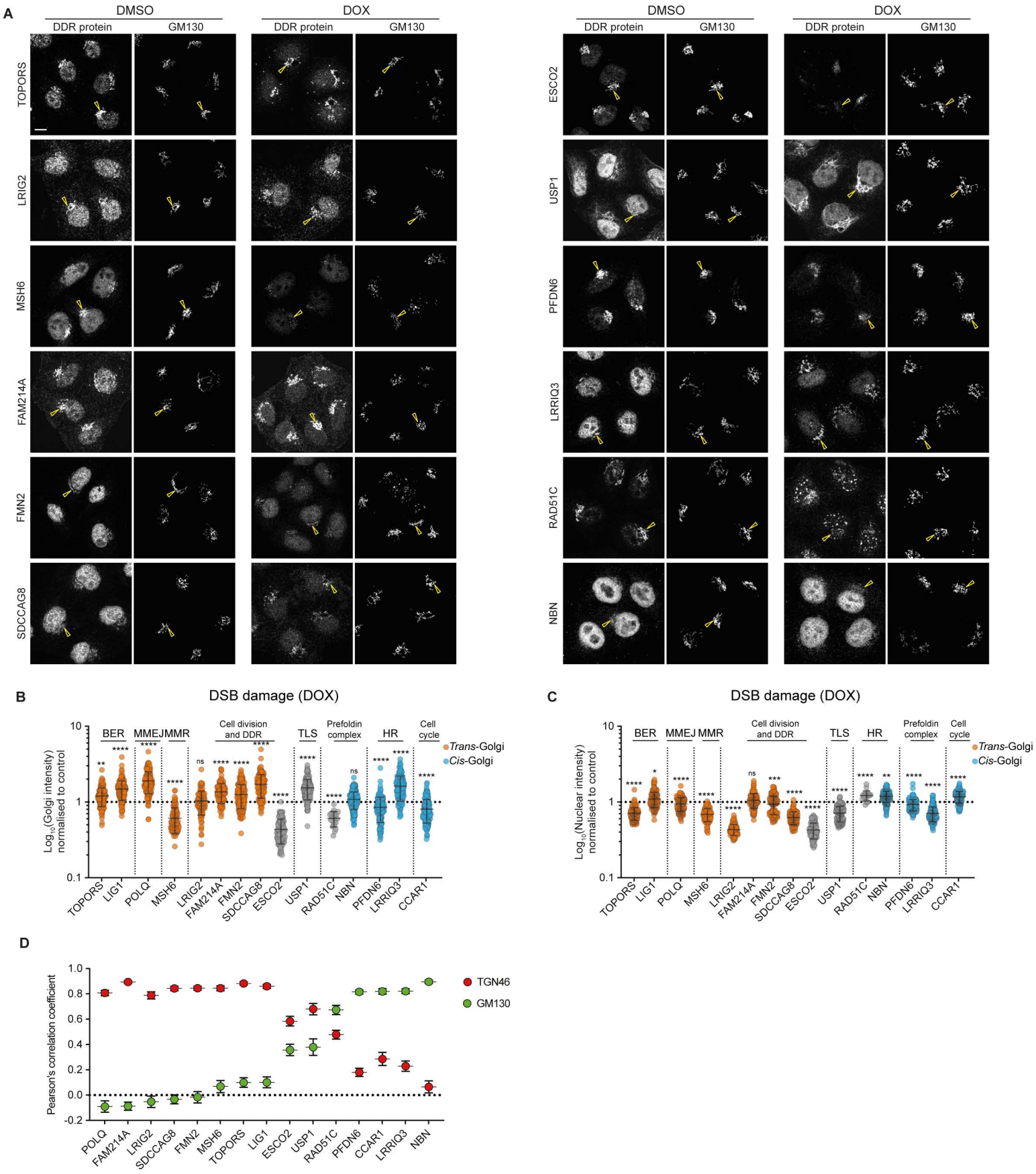

Fig. S3. (**A**) Representative images of HK cells were stained with antibodies against DDR proteins and the Golgi marker, GM130. HK cells were treated with DOX (40 μM, 3 h), fixed and stained with antibodies against DDR proteins and the Golgi marker, GM130 (**A** to **C**); yellow arrows denote the Golgi membranes. Scale bar, 10 μm. Quantification of the relative intensity of DDR proteins at the Golgi **(B)** and the nucleus (**C**) DOX treated normalised to untreated control. Data represent the mean ± s.e.m. (n = 3 biologically independent samples with at least 200 cells analysed for each protein in control and treatment conditions). The proteins are classified according to their Golgi localisation patterns **(Fig. 2E)**. Statistical significance was determined using a two-tailed unpaired Student's t-test; ns P > 0.05, **P < 0.01, ***P < 0.001, ****P <0.0001, compared to untreated control. (**D**) Golgi-cisternal localisation analysis of Golgi-nuclear DDR proteins. HK cells were treated with Nocodazole (33 μM, 3 h), fixed and stained with antibodies against DDR proteins. Quantification of Pearson's correlation coefficient (PCC) between *cis*-Golgi and *trans*-Golgi markers and DDR proteins; N ≥ 4 cells; n ≥ 36 mini stacks.

SUPPLEMENTARY FIGURE 4

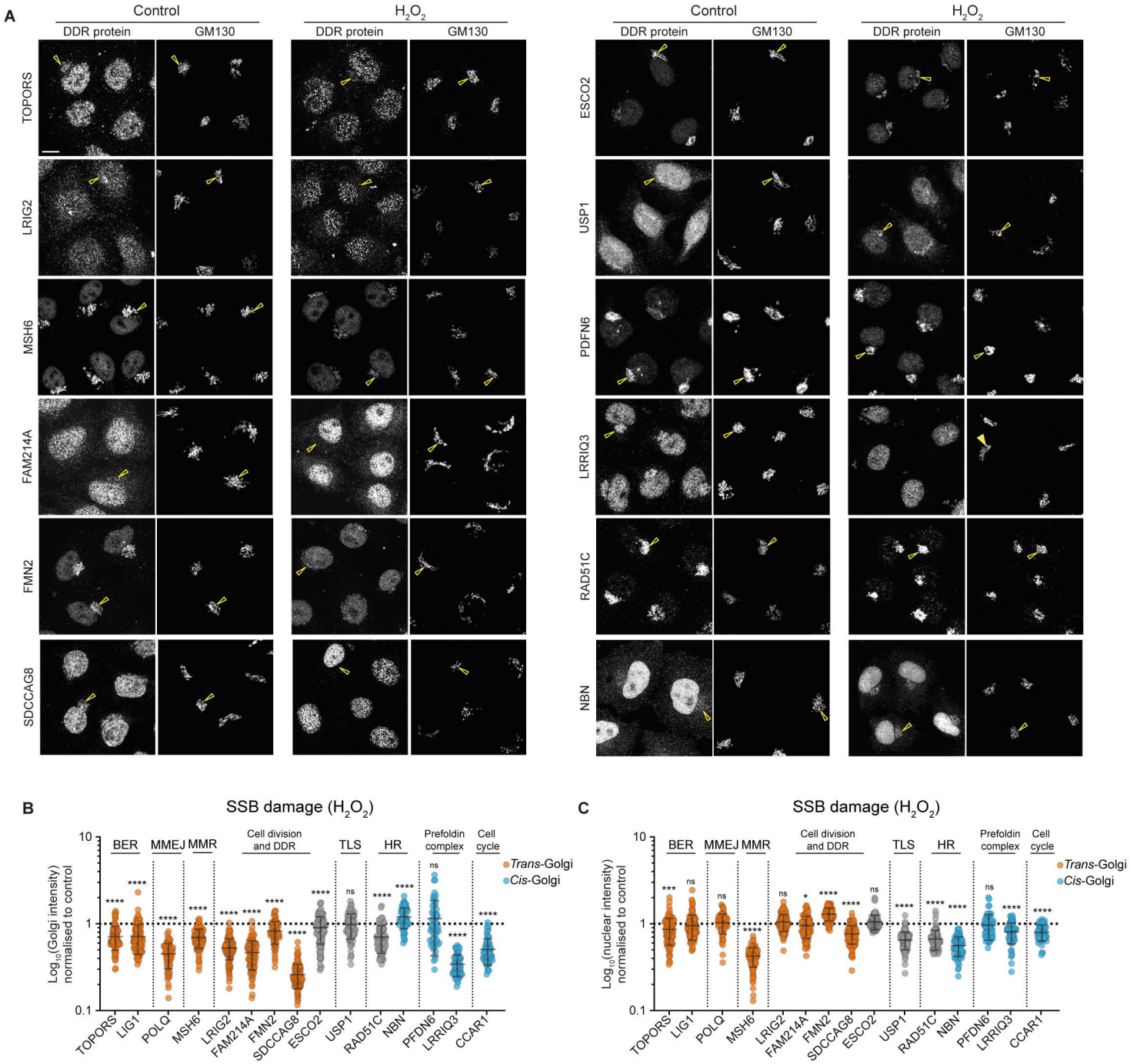

Fig. S4. (**A**) Representative images of HK cells were stained with antibodies against DDR proteins and the Golgi marker, GM130. HK cells were treated with H_2O_2 (50 µM, for 20 min followed by 15 min recovery), fixed and stained with antibodies against DDR proteins and the Golgi marker, GM130 (**A** to **C**); yellow arrows denote the Golgi membranes. Scale bar, 10 µm. Quantification of the relative intensity of DDR proteins at the Golgi (**B**) and the nucleus (**C**) H_2O_2 treated normalised to untreated control. Data represent the mean ± s.e.m. (n = 3 biologically independent samples with at least 200 cells analysed for each protein in control and treatment conditions). The proteins are classified according to their Golgi localisation patterns **(Fig. 2E)**. Statistical significance was determined using a two-tailed unpaired Student's t-test; ns P > 0.05, **P < 0.01, ***P < 0.001, ****P <0.0001, compared to untreated control.

SUPPLEMENTARY FIGURE 5

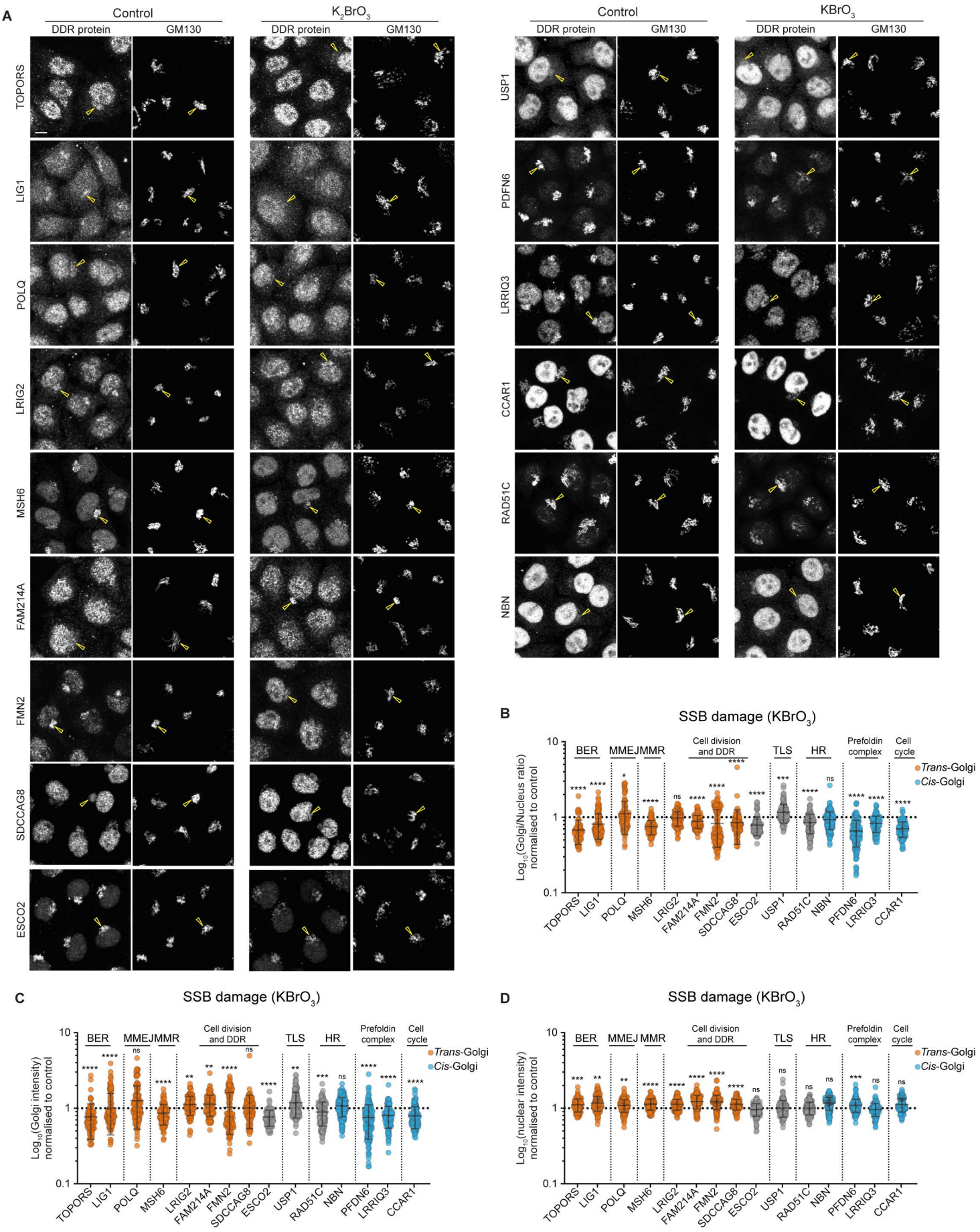

Fig. S5. (**A**) Representative images of HK cells were stained with antibodies against DDR proteins and the Golgi marker, GM130. HK cells were treated with $KBrO_3$ (5 mM, 3h), fixed and stained with antibodies against DDR proteins and the Golgi marker, GM130 (**A** to **D**); yellow arrows denote the Golgi membranes. Scale bar, 10 µm. (**B**) A ratio of DDR protein Golgi-nuclear distribution after treatment with $KBrO_3$. Quantification of the relative intensity of DDR proteins at the Golgi (**C**) and the nucleus (**D**) KBrO3 treated normalised to untreated control. Data represent the mean ± s.e.m. (n = 3 biologically independent samples with at least 200 cells analysed for each protein in control and treatment conditions). The proteins are classified according to their Golgi localisation patterns **(Fig. 2E)**. Statistical significance was determined using a two-tailed unpaired Student's t-test; ns P > 0.05, **P < 0.01, ***P < 0.001, ****P <0.0001, compared to untreated control.

SUPPLEMENTARY FIGURE 6

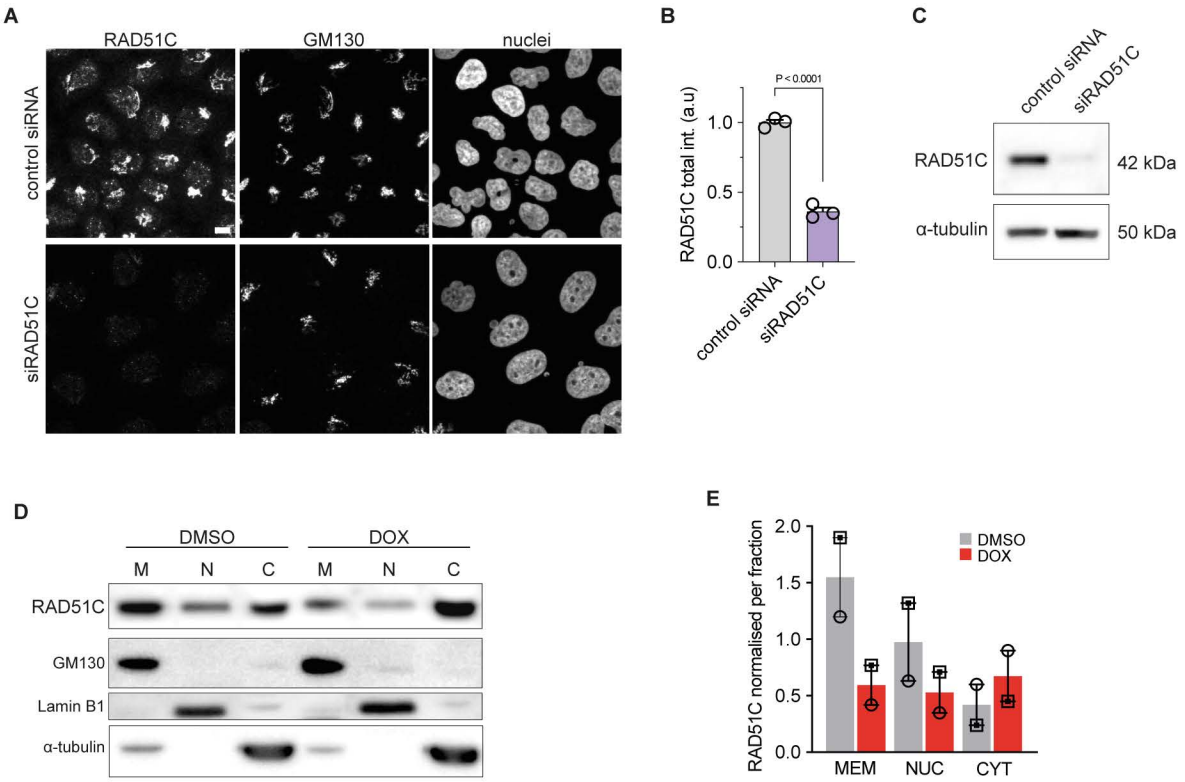

Fig. S6. (**A**) Representative images showing the RAD51C antibody specificity. HK cells were stained with antibodies against RAD51C and GM130; DNA was stained with Hoechst 33342. (**B**) Quantification of RAD51C sum intensity after RAD51C depletion. Data represent the mean ± s.e.m. (n = 3 biologically independent samples with a total of 831 cells analysed). (**C**) Western blot analysis showing the level of RAD51C protein level, in RAD51C-depleted and control cells (n = 3 biologically independent samples). Statistical significance was determined using a two-tailed unpaired Student's t-test. (**D**) Western blot showing the subcellular localisation of RAD51C treated with the DMSO and doxorubicin. The protein levels normalised against the respective fraction control ($RAD51C^{mem}$/GM130; $RAD51C^{nuc}$/Lamin B1; $RAD51C^{cyt}$/alpha-tubulin). Data represent the mean ± s.e.m; (n = 2 biologically independent samples). (**E**) Quantification of RAD51C membrane-nuclear distribution ratio after treatment with DOX, calculated from isolated fractions.

SUPPLEMENTARY FIGURE 7

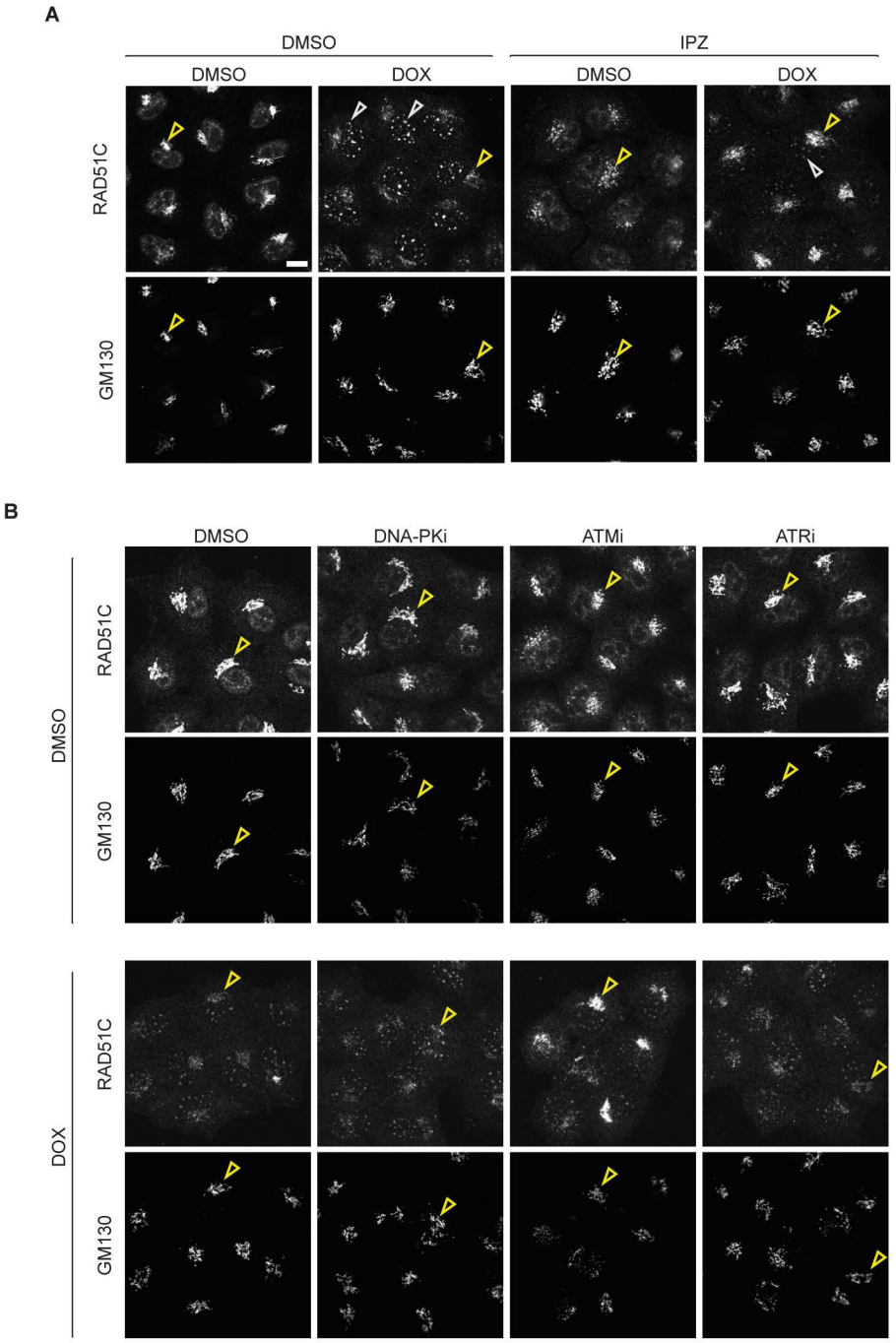

Fig. S7. Representative images of HK cells were stained with antibodies against RAD51C and GM130. (**A**) Cells were treated with DMSO or IPZ prior to a 3-hour treatment with DOX. (**B**) HK cells were treated with DMSO (control) alone or with ATM inhibitor (KU55933), ATR inhibitor (VE-821) or DNA-PK inhibitor (NU7441) prior to a 3-hour treatment with doxorubicin. Yellow arrows denote the Golgi membrane; white denotes nuclear foci. Scale bars, 10 μm.

SUPPLEMENTARY FIGURE 8

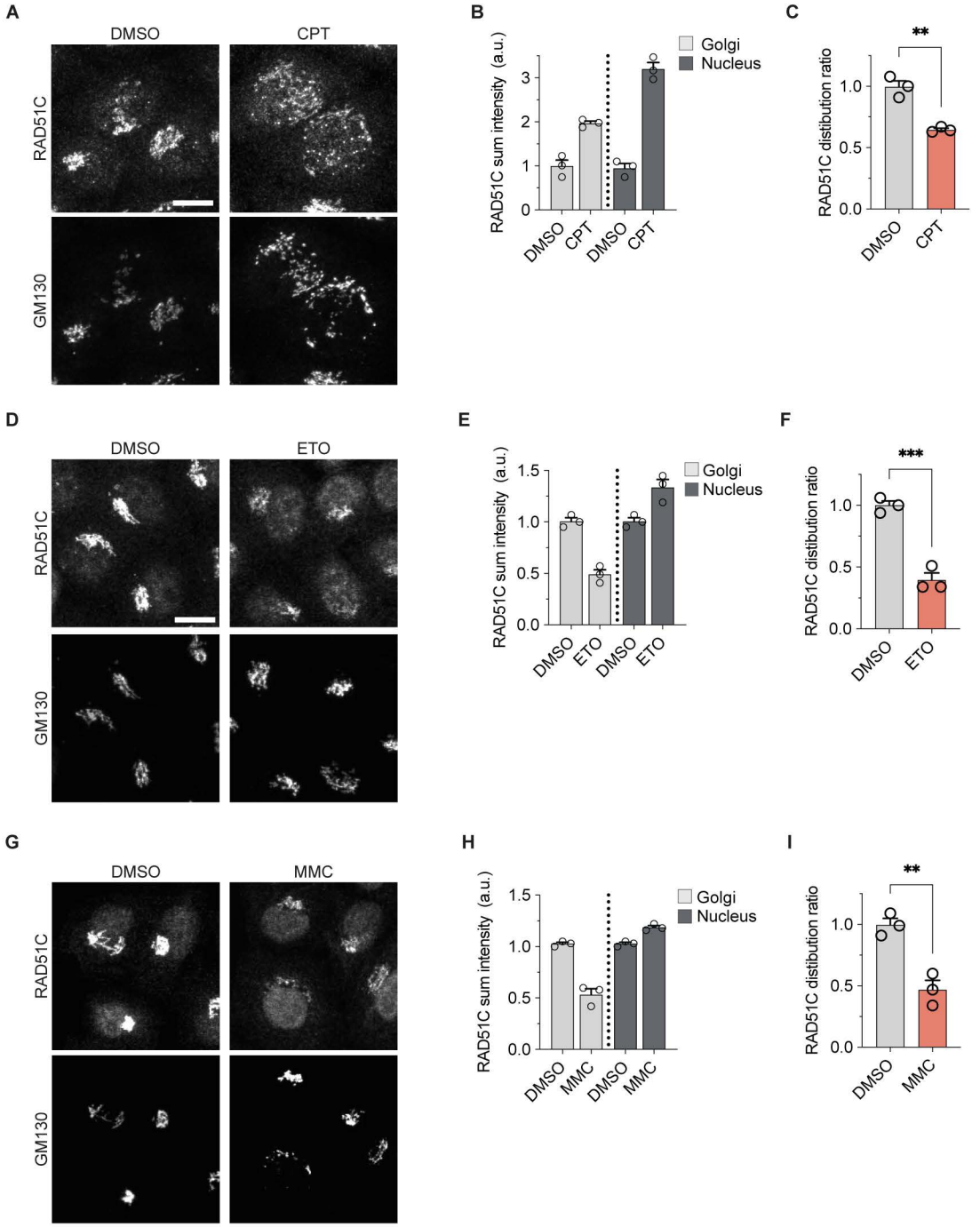

Fig. S8. HK cells stained with antibodies against RAD51C and GM130. Cells were treated with (**A**) Camptothecin (CPT), (**D**) etoposide (ETO) and (**G**) mitomycin C (MMC) for 16 h followed by media change for 2 h; scale bar 10 µm. Quantification of RAD51C distribution between the Golgi and nuclear compartment after (**B**) CPT, (**E**) ETO and (**H**) MMC treatments. Quantification of RAD51C distribution between the Golgi and nuclear compartment after (**C**) CPT, (**F**) ETO and (**I**) MMC treatments. Data represent the mean ± s.e.m. (n = 3 biologically independent samples with more than 600 cells analysed per treatment). Statistical significance was determined using a two-tailed unpaired Student's t-test. **P<0.01; ***P<0.001.

SUPPLEMENTARY FIGURE 9

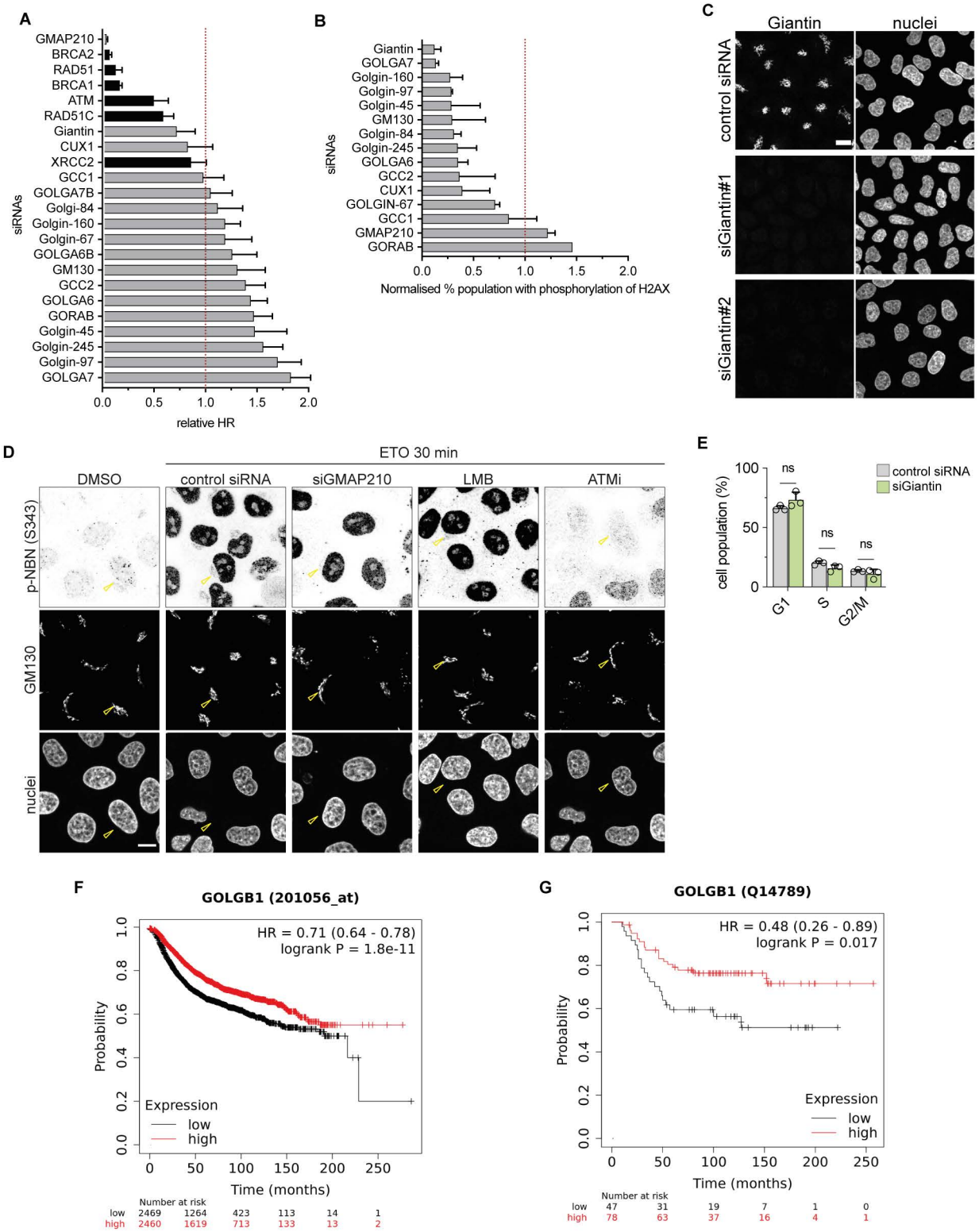

Fig. S9. (**A**) siRNA screen data (Adamson et al. 2012) showing the relative homologous recombination (HR) repair rate upon systematic knockdown of the Golgin protein family (grey) and HR complex proteins (black). (**B**) siRNA screen data (Paulsen 2010) showing the relative percent cell population with phosphorylation of H2AX upon systematic knockdown of the Golgins. The datasets are normalised to the negative control set at 1. (**C**) HK cells were transfected with control, or Giantin siRNAs for 72 hours. The cells were stained with antibodies against Giantin and nuclei were stained with Hoechst 33342; scale bar 10 µm. (**D**) HK cells stained with antibodies against pNBN (s343) and GM130. Various treatments were applied to the cells: GMAP210 knockdown, ATM inhibitors, and leptomycin B (LMB) to block nuclear export. These treatments were conducted under both control conditions and following a 30-minute induction of DNA damage using etoposide. (**E**) Cell cycle profile of HK cell treated with Giantin or control siRNA. Data represent the mean ± s.e.m. (n = 3 biologically independent samples). (**F** and **G**) Kaplan-Meier survival plots in patients with high and low mRNA (f) (Győrffy 2021) and protein (g) (Ősz, Lánczky, and Győrffy 2021) Giantin expression in Breast Cancer patients. The graph was generated using the kmplot database (https://kmplot.com).

SUPPLEMENTARY FIGURE 10

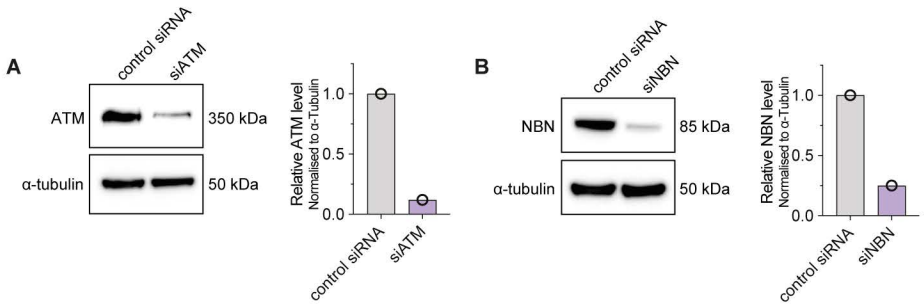

Fig. S10. Western blot analysis showing the level of proteins in siRNA-depleted and control cells for the validation of antibody specificity for (**A**) ATM and (**B**) NBN. The changes in protein level were quantified as relative protein level normalised to alpha-tubulin.